

COMPARING SIMULATED HYDROLOGIC RESPONSE BEFORE AND AFTER
THE 2011 BASTROP COMPLEX WILDFIRE

By

Victoria G. Stengel, B.S.

A thesis submitted to the Graduate Council of
Texas State University in partial fulfillment
of the requirements for the degree of
Master of Science
with a Major in Geography
May 2014

Committee Members:

T. Edwin Chow, Chair

Jennifer Jensen

Richard Earl

COPYRIGHT

by

Victoria G. Stengel

2014

FAIR USE AND AUTHOR'S PERMISSION STATEMENT

Fair Use

This work is protected by the Copyright Laws of the United States (Public Law 94-553, section 107). Consistent with fair use as defined in the Copyright Laws, brief quotations from this material are allowed with proper acknowledgement. Use of this material for financial gain without the author's express written permission is not allowed.

Duplication Permission

As the copyright holder of this work I, Victoria G. Stengel, authorize duplication of this work, in whole or in part, for educational or scholarly purposes only.

DEDICATION

This work is dedicated to the memory of

Mrs. Freddy M. Magee

and to

David Gray

Thank you for encouraging me to pursue a college education.

ACKNOWLEDGEMENTS

Thank you to my advisor Dr. T. Edwin Chow for encouraging my thesis research interests, and for expanding the scope of my research interests. Thank you for tirelessly advising me through my Master's degree, and the thesis process.

Thank you to my thesis committee Dr. Jennifer Jensen, and Dr. Richard Earl for your support and guidance through the thesis process.

I would also like to thank Dr. Chow, Dr. Jensen, and Dr. Earl for their individual and collective encouragement to pursue my intellectual interests throughout my undergraduate and graduate studies. Their guidance proved to be invaluable in leading me to achieve a graduate education, and for this I am infinitely grateful.

I would like to thank Allison Glass-Smith, Daniel Pearson, Florence Thompson, Johnathan Bumgarner, Joseph Vrabel, Justin McCreight, Meghan Roussel, Michael Canova, Oliver Jensen, Sally Holl, and Thomas Burley for their support throughout the thesis process.

TABLE OF CONTENTS

	Page
ACKNOWLEDGEMENTS	v
LIST OF TABLES	viii
LIST OF FIGURES	x
ABSTRACT.....	xiii
CHAPTER	
1. INTRODUCTION	1
1.1 The Bastrop Complex Wildfire.....	1
1.2 Fire Impacts on Surface Hydrology	5
1.3 Thesis Purpose	6
2. LITERATURE REVIEW	7
2.1 Fire Impacts on Watershed Landscape	7
2.1.1 Fire Impacts on Surface Runoff.....	8
2.1.2 Fire Impacts on Erosion and Sediment Yield	11
2.2 The Roles of GIS and Remote Sensing.....	13
2.3 The Soil and Water Assessment Tool (SWAT) Model	15
2.4 Summary	17
3. METHODOLOGY	19
3.1 Research Questions	19
3.2 Study Area	19
3.3 Data.....	21
3.4 SWAT Model.....	22

3.4.1 Calibration.....	26
3.4.2 Statistical Analysis.....	29
4. RESULTS	31
4.1 LCLU Classification	31
4.2 SWAT Model.....	37
4.2.1 Continuous simulation of the study area.....	38
4.2.2 Discrete events extracted from the continuous simulation of the study area	39
4.2.3 Simulation at Subbasin 4	51
5. DISCUSSION	59
5.1 LCLU Change	60
5.2 Hydrology	61
5.2.1 Surface Runoff	61
5.2.2 Peak Discharge.....	63
5.2.3 Time to Peak	64
5.2.4 Sediment	65
5.2.5 Comparing the Calibration and the Validation Period Simulation Results	67
5.3 Limitations	68
6. CONCLUSION.....	71
6.1 Future Research Opportunities	72
7. LITERATURE CITED	73

LIST OF TABLES

Table	Page
1. Calibration and validation objective function results	28
2. LCLU change from August and October 2011 for the study area.....	33
3. LCLU change from August and October 2011 for subbasin 4.....	34
4. LCLU classification error matrix for August 2011.....	35
5. LCLU classification error matrix for October 2011	36
6. Study area simulation totals for pre- and post-fire peak rainfall intensity, time to peak (T_p), peak discharge (Q_p), runoff volume, and sediment volume for the 30 mm (1.2 in) rain event	39
7. Study area simulation totals for pre- and post-fire peak rainfall intensity, time to peak (T_p), peak discharge (Q_p), runoff volume, and sediment volume for the 50 mm (2 in) rain event	42
8. Study area simulation totals for pre- and post-fire peak rainfall intensity, time to peak (T_p), peak discharge (Q_p), runoff volume, and sediment volume for the 80 mm (3 in) rain event	45
9. Study area simulation totals for pre- and post-fire peak rainfall intensity, time to peak (T_p), peak discharge (Q_p), runoff volume, and sediment volume for the series of rain events	48
10. Subbasin 4 simulation totals for pre- and post-fire peak rainfall intensity, time to peak (T_p), peak discharge (Q_p), runoff volume, and sediment volume for the 31 mm (1.22 in) rain event.	51
11. Subbasin 4 simulation totals for pre- and post-fire peak rainfall intensity, time to peak (T_p), peak discharge (Q_p), runoff volume, and sediment volume for the 55 mm (2.15 in) rain event.....	53

12. Subbasin 4 simulation totals for pre- and post-fire peak rainfall intensity, time to peak (T_p), peak discharge (Q_p), runoff volume, and sediment volume for the 83 mm (3.29 in) rain event	55
13. Subbasin 4 simulation totals for pre- and post-fire peak rainfall intensity, time to peak (T_p), peak discharge (Q_p), runoff volume, and sediment volume for the multimodal rain event	57

LIST OF FIGURES

Figure	Page
1. Drought conditions for September 2011 (Source: NDMC, 2011)	3
2. The Bastrop Complex Wildfire burn severity classification (Source: TPWD, 2011)	4
3. The study area–drainage area for the Colorado River stream segment between the USGS streamgaging-stations at Bastrop and Smithville, TX.....	20
4. A Landsat 5 image (RGB432) on September 11, 2011, showing the Bastrop Complex Wildfire burn scar within the study area.....	21
5. Observed streamflow and precipitation in the study area from July 2004 To December 2010.....	22
6. Scatter plot diagram comparing observed to simulated daily streamflow values.....	29
7. Data-Flow Diagram	30
8. August pre-fire LCLU classification.....	32
9. October post-fire LCLU classification.....	32
10a. Water yield generated by a 31 mm (1.22 in) rain event for the calibration period	40
10b. Sediment yield generated by a 31 mm (1.22 in) rain event for the calibration period	40
11a. Water yield generated by a 27 mm (1.06 in) rain event for the validation period	41
11b. Sediment yield generated by a 27 mm (1.06 in) rain event for the validation period	41

12a. Water yield generated by a 55 mm (2.15 in) rain event for the calibration period	43
12b. Sediment yield generated by a 55 mm (2.15 in) rain event for the calibration period	43
13a. Water yield generated by a 51 mm (2.01 in) rain event for the validation period	44
13b. Sediment yield generated by a 51 mm (2.01 in) rain event for the validation period	44
14a. Water yield generated by an 83 mm (3.29 in) rain event for the calibration period	46
14b. Sediment yield generated by an 83 mm (3.29 in) rain event for the calibration period	46
15a. Water yield generated by a 76 mm (3 in) rain event for the validation period	47
15b. Sediment yield generated by a 76 mm (3 in) rain event for the validation period	47
16a. Water yield generated by 25 mm (1 in), 26 (1.01 in), and 42 (1.66 in) rain events for the calibration period	49
16b. Sediment yield generated by 25 mm (1 in), 26 (1.01 in), and 42 (1.66 in) rain events for the calibration period	49
17a. Water yield generated by 32 mm (1.25 in), 13 mm (0.5 in), 13 mm (0.52 in) rain events for the validation period.....	50
17b. Sediment yield generated by 32 mm (1.25 in), 13 mm (0.5 in), 13 mm (0.52 in) rain events for the validation period	50
18a. Water yield generated by a 31 mm (1.22 in) rain event for the calibration period	52
18b. Sediment yield generated by a 31 mm (1.22 in) rain event for the calibration period	52
19a. Water yield generated by a 55 mm (2.15 in) rain event for the calibration period	54

19b. Sediment yield generated by a 55 mm (2.15 in) rain event for the calibration period	54
20a. Water yield generated by an 83 mm (3.29 in) rain event for the calibration period	55
20b. Sediment yield generated by an 83 mm (3.29 in) rain event for the calibration period	56
21a. Water yield generated by 25 mm (1 in), 26 mm (1.01 in), 42 (1.66 in) rain events for the calibration period	57
21b. Sediment yield generated by 25 mm (1 in), 26 mm (1.01 in), 42 (1.66 in) rain events for the calibration period	58

ABSTRACT

On September 4, 2011, the Bastrop Complex Wildfire grew into what would become the most destructive wildfire in the history of Texas. The fire consumed approximately 130 square kilometers of wildland urban interface near Bastrop, TX. The Loblolly Pine trees of the Lost Pine Forest suffered high rates of tree mortality. At the time the region was experiencing one of the driest and hottest periods of record in Texas history.

The purpose of this study was to explore possible changes in surface hydrology caused by the Bastrop Complex Wildfire. This study used multispectral remote sensing imagery acquired from Landsat 5 immediately before, and after the wildfire to classify land cover/land use (LCLU) change within the drainage area of the Colorado River where the wildfire occurred. The drainage area was defined by the upstream and downstream USGS streamgaging-stations along the Colorado River. The LCLU data were applied to the Soil Water Assessment Tool (SWAT) in order to simulate pre- and post-fire surface hydrology conditions. The resulting simulations were compared to examine possible changes in surface runoff volume and sediment yield for the continuous time simulation and for discrete rainfall events of varying magnitudes.

The comparison of the continuous time simulation resulted in a significant increase in post-fire surface runoff and sediment yield. Despite the fact that there were no significant differences of water yield and time to peak among discrete rainfall events, it was found that the peak discharge increases with higher rainfall intensity. This research also reported a large percent increase in post-fire sediment yield for the discrete rain events that is consistent with the literature.

1. INTRODUCTION

1.1 The Bastrop Complex Wildfire

On the afternoon of September 4, 2011, a moisture-stressed pine forest of Bastrop County located in central Texas ignited and grew into one of the most destructive wildfires in the history of Texas and the United States—the Bastrop Complex Wildfire. The wildfire devastated 32,000 acres of land, and 1,723 commercial and residential structures. It occurred in an area of pine forest north and east of the city of Bastrop, Texas. The area was vulnerable to wildfire due to climatic conditions in the wildland urban interface (WUI) (Ridenour *et al.*, 2012).

The Bastrop Complex Wildfire fire began in a belt of isolated coniferous forest located within a post oak savanna ecological region in Bastrop County, Texas. This Loblolly Pine (*Pinus taeda*) forest is known as the Lost Pine Forest. The isolated group is a pine species that is abundant throughout the southeastern United States, and is thought to have been separated during the last ice age. The Lost Pine Forest Loblolly Pines are a drought tolerant variety of the abundant Loblolly Pine species (Rahman *et al.* 2003). Additional tree varieties in the study area include Ashe Juniper (*Juniperus ashei*), and Oak varieties (e.g., *Quercus virginiana*, *Quercus macrocarpa*).

The climate conditions created an environment that was vulnerable to wildfire: low moisture content, low humidity, and high temperatures. In the spring and summer of 2010, wetter than average conditions promoted the growth of vegetation. By October 2010, drier than average conditions had started to stress the abundant vegetation. However, by 2011, the majority of the state, including Bastrop County, was experiencing an exceptional drought

(Ridenour *et al.*, 2012) along with record high temperatures throughout the summer. The month of August proved to be the single hottest month reported in Texas history. By September of 2011, Texas had experienced the 12 driest consecutive months on record and more than 80% of the state was classified as exceptional drought (Figure 1) (NDMC, 2011). The Texas Forest Service rated Bastrop County vegetation as extremely dry based on the Fuel Dryness Index, an index that assesses wildfire risk. From November of 2010 to October of 2011 more than 16,200 square kilometers burned throughout Texas.

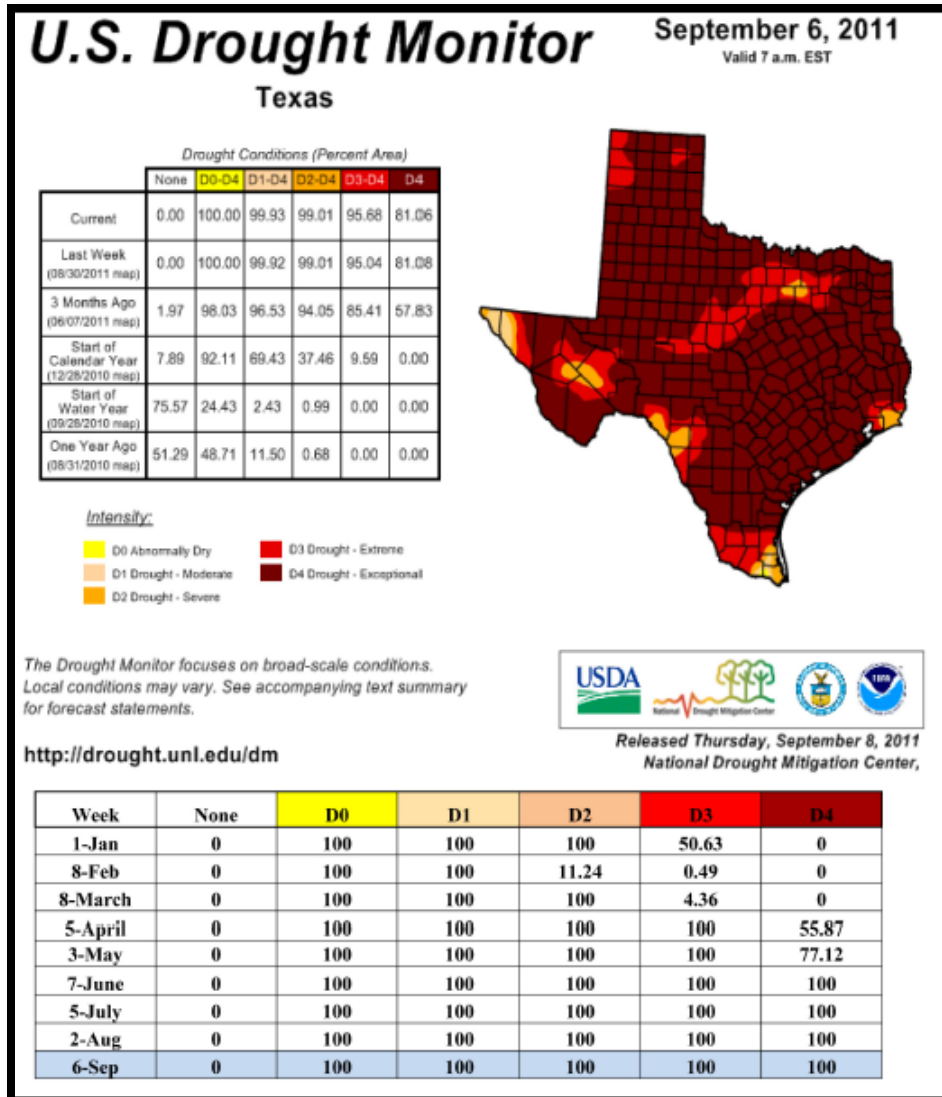


Figure 1. Drought conditions for September 2011 (Source: NDMC, 2011).

In September 2011, Tropical Storm Lee pushed strong dry northeastern winds across the state of Texas from the coast of Louisiana, causing the relative humidity to drop. On Sunday, September 4, 2011, 57 fires ignited across Texas (Ridenour *et al.*, 2012). At approximately 2:20 pm the first of the three fires that would grow into the Bastrop Complex Wildfire (Figure 2) ignited due a downed power line (Ridenour *et al.*,

2012). The fire immediately grew out of control. The local sheriff's department began the evacuation of the area 13 minutes after emergency response was first notified of the fire. By September 27, the fire was 98% contained; the fire was confirmed extinguished on October 9 (Ridenour *et al.*, 2012).

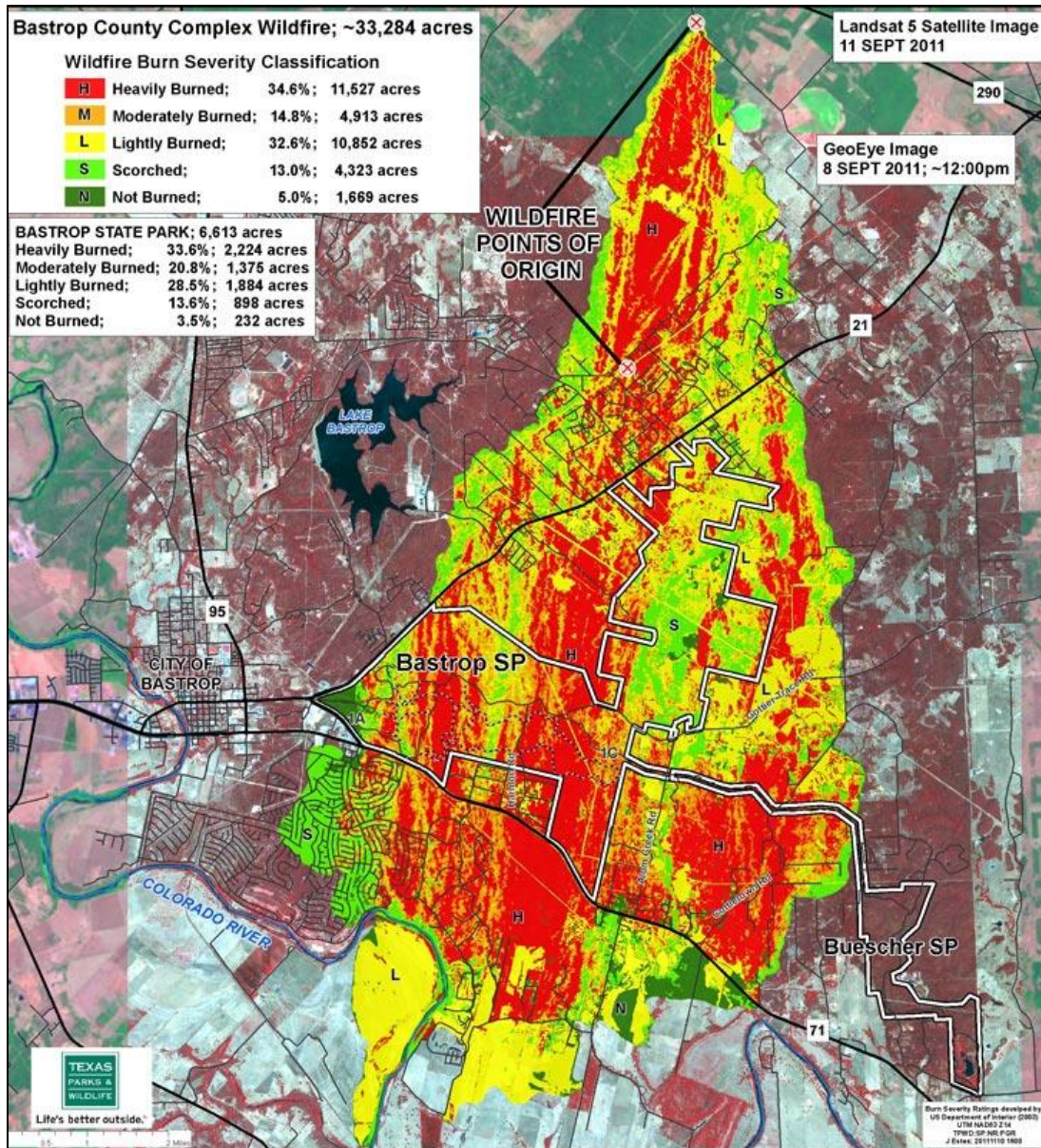


Figure 2. The Bastrop Complex Wildfire burn severity classification (Source: TPWD, 2011).

Many structures in the low density residential areas were damaged by the intense fire. It was estimated that the Loblolly Pine forest produced approximately 85% of the fuel for the fire. Agriculture and grassland accounted for 10% of the burned area, 4% of the burned area was riparian, and the remaining 1% of the burned area was undeveloped land (Ridenour *et al.*, 2012).

1.2 Fire Impacts on Surface Hydrology

Fire has many effects on surface hydrology—a complex dynamic system in which the behavior of many of the components, including precipitation, evaporation, interception, ground water absorption, and surface runoff, are determined by climatic, geological, and ecological controls. Perturbations of the individual components could result in changes in surface hydrology for a watershed throughout the fire recovery process.

As a result of wildfire, the loss of vegetation cover reduces interception and increases surface water runoff from rain events (i.e., storm flow). The reduction in vegetation ground cover also leaves soil exposed and reduces storm flow friction. Burned organic material littered along a forest floor could result in a charred layer of top soil. Dense charred soil and deposits of ash decrease soil permeability in the months following a fire (Kunze and Stednick, 2006). Over time soil loosens and soil permeability gradually returns to pre-fire conditions. However, the lack of organic material in top soil and decaying root structures at various depths reduces soil cohesion. Ultimately, the combination of these factors has the potential to change storm flow behavior during the

fire recovery process, resulting in flashier floods, increased erosion, channel degradation, higher debris flows, and the overall deterioration of water quality within a watershed.

Fire plays an important role in maintaining the health of many coniferous forest ecosystems. However, extreme fires have the potential to result in greater amounts of vegetation loss and tree mortality (Kunze and Stednick, 2006; Townsend and Douglas, 2000). Longer periods of vegetation recovery leave a watershed vulnerable to permanent geomorphic changes (Gartner *et al.*, 2008; Shakesby, 2005). Changes in geomorphology and vegetation have the potential to alter the dynamics of hydrology, ecological health (Kunze and Stednick, 2006; Townsend and Douglas, 2000) and damage life, and property within a watershed (Doerr and Shakesby, 2006).

1.3 Thesis Purpose

The primary objective of this study was to examine the change in surface hydrology caused by the September 2011 Bastrop Complex Wildfire in Bastrop County, Texas. The study used pre- and post-fire multispectral imagery to quantify land cover change caused by the wildfire. The study compared pre- and post-fire surface hydrology simulations of the drainage area where the burn scar occurred. The Soil and Water Assessment Tool (SWAT) model was used to simulate hydrologic components (e.g., evapotranspiration (ET), soil infiltration, interception).

2. LITERATURE REVIEW

2.1 Fire Impacts on Watershed Landscape

Wildfire changes the dynamic of the hydrologic system of a watershed. The level of interruption depends on the frequency, intensity, and spatial extent of the fire damage and the physical characteristics of the watershed, e.g., slope, land use, land cover, the percentage of burned vegetation, and vegetation recovery time (Kinoshita and Hogue, 2011; Kunze and Stednick, 2006; Townsend and Douglas, 2004; Townsend and Douglas 2000). Disturbances caused by wildfire can lead to an increase in surface water yield, stream channel erosion, and the overall deterioration of water quality in a watershed.

In general, vegetation loss decreases interception, infiltration, and evapotranspiration (Kunze and Stednick, 2006; Townsend and Douglas, 2000). Fire has a tendency to affect riparian vegetation differently than upland vegetation, because of differences in soil moisture, microclimates, geomorphology, vegetation composition, and vegetation structure (Dwire and Kauffman, 2003). The upland vegetation is affected by fire more frequently and severely than riparian vegetation, although differences in burn severity and frequency varies by region and forest type (Dwire and Kauffman, 2003).

Intensive wildfires that consume high volumes of vegetation can leave the undergrowth of a forest canopy barren and cause tree mortality (Kunze and Stednick, 2006; Townsend and Douglas, 2000). Hot fires fueled by dense undergrowth and organic material accumulated on the forest floor and mixed in top soil have the ability to transform permeable top soils into a dense layer of charred material. Charred top soil decreases ground water absorption and increases surface runoff (Kinoshita and Hogue,

2011; Gartner *et al.*, 2008; Kunze and Stednick, 2006). The recovery of the infiltration rate of water repellent soil varies depending on the severity of the fire. Kunze and Stednick (2006) reported that soil repellency played an important role in surface water runoff rates in the months following a fire in a watershed located in the Colorado Rocky Mountains. Areas of water repellent soil had fully recovered after one year, and for severely burned areas, infiltration rates increased by 50% after one year.

Ash deposition has the potential to affect both water quality and quantity of surface hydrology. The impact of ash on surface hydrology varies depending on wind dispersion of ash deposits and soil retention of ash (Townsend and Douglas, 2004). Ash deposits expand when wetted and reduces soil porosity. Thus, ash deposition contributes to soil impermeability and sediment yield (Kunze and Stednick, 2006; Gartner *et al.*, 2008).

2.1.1 Fire Impacts on Surface Runoff

Destructive wildfire creates the potential for more intense, flashier floods than the watershed experienced before a destructive wildfire. Watersheds that have been damaged by fire have experienced increases in instantaneous peak discharge by several hundred times compared to pre-fire rates in undamaged watersheds (Friedel, 2011; Kunze and Stednick, 2006; Scott, 1993). Intensity of streamflow depends on the timing of rain events during the watershed recovery process (Ryan *et al.*, 2011; Kunze and Stednick, 2006). The intensity of water yield and peak discharge decreases over time as the forest regenerates (Kunze and Stednick, 2006).

Changes in surface flow dynamics are a product of many factors, including vegetative coverage, soil repellency, soil type, etc. (Scott, 1993). Destructive wildfires can affect stream discharge in terms of increased flow volume and velocity (Kinoshita and Hogue, 2011; Ryan *et al.*, 2011; Cannon *et al.*, 2008, Gartner *et al.*, 2008; Kunze and Stednick, 2006; Scott, 1993; Loaiciga *et al.*, 2001); swifter moving water has the potential to change the time to peak for storm flow. Vegetation loss decreases evapotranspiration, interception and groundwater absorption (Kunze and Stednick, 2006; Townsend and Douglas, 2004). Townsend and Douglas (2004) reported that the increase in surface runoff is approximately proportional to the ratio of vegetation loss within a watershed. Biomass usually contributes to the debris and litter on ground, and hence vegetation loss also reduces surface roughness which could lead to swifter moving water (Ryan *et al.*, 2011). Soil repellency reduces ground water infiltration (Kunze and Stednick, 2006, Scott, 1993), and therefore is a contributor to surface runoff.

Scott (1993) compared surface runoff of four burned catchments in South Africa. Two catchments were primarily composed of pine and Eucalyptus forest; the other two catchments were composed of shrub. Scott observed minimal change for the shrub catchments. For the forested catchments he observed a 290% and 1110% increase in peak discharge, and a 201% and 92% for quick-flow volume as a result of soil repellency.

Loaiciga *et al.* (2001) examined 10 wildfires in the Malibu Creek watershed in Malibu, California. The 272 square kilometer watershed consists of chaparral forest. The 10 wildfires consumed varying areas of land, ranging from 4-46% of the watershed. The study concluded that streamflows increased 20-30% for fire years compared to non-fire

years. A fire that consumed 40% of the watershed could result in a 30% increase in surface water yields at the outlet.

Kunze and Stednick (2006) compared the surface water yields of two watersheds near Drake, Colorado that were damaged by the 2000 Bobcat wildfire. The Bobcat Gulch watershed area is 2 square kilometers (0.8 square miles). The watershed was treated for surface runoff and erosion control; the Jug Gulch watershed area is 3.9 square kilometers (1.5 square miles) and was untreated. Both watersheds experienced 100% fire damage; however, the severity of the fire damage varied across the watersheds. Kunze and Stednick (2006) found that the two watersheds were sensitive to precipitation intensity, which was found to be associated with 86% of variability in peak discharge, 76% of variability in storm runoff, and greater than 80% of variability in sediment yield. Kunze and Stednick (2006) also compared the characteristics of surface hydrology in neighboring watersheds that experienced minimal or no fire damage. The damaged watersheds produced water yields that were an order of magnitude greater than what was probably experienced during pre-fire conditions (Kunze and Stednick, 2006). They concluded that the watershed was most susceptible to increased surface water yields during the two years following the fire because water repellent top soil recovered to pre-fire absorption rates after one year, and vegetation coverage recovered after two years.

Kinoshita and Hogue (2011) studied post-fire vegetation recovery and resilience in the San Bernardino Mountains of Southern California. They looked at two arid Mediterranean climate watersheds that were both composed of chaparral and mixed forest in the higher elevations and coastal sage scrub in the lower elevations. They stated that both surface runoff and baseflow were higher after the wildfire. During the

vegetation recovery process in these arid watersheds, vegetation would grow during wet seasons and senesce during the dry season. The authors specifically state that grasses would need to establish deep root systems in order to survive the dry seasons. They observed seasonal variability in the behavior of the watershed hydrology. After seven years, parts of the watershed fully recovered, while other parts had not yet established perennial vegetation. Lack of full vegetation recovery was observed primarily for pixels that indicated a high burn severity and steep slopes.

2.1.2 Fire Impacts on Erosion and Sediment Yield

Post-fire erosion can be destructive. In the WUI sediment redistribution can cause damage to property, and infrastructure (Doerr and Shakesby, 2006). Sediment redistribution also plays a functional role in riparian ecosystems (Benda *et al.*, 2003). Increasing water yield provides more energy for erosion, leading to increasing sediment yield. Heavy sediment loads, ash, charcoal, and other minerals captured by surface water runoff lead to deteriorated water quality (Ouyang *et al.*, 2010; Ryan *et al.*, 2011; Townsend and Douglas, 2004; Townsend and Douglas, 2000). Erosion from overland flows, and stream channel degradation produce high sediment yields (Friedel, 2011). The combustion of organic material in soil and the breakdown of root structures over time reduce soil cohesion, which can result in erosion and debris flows (Friedel, 2011; Kunze and Stednick, 2006). The magnitude of sediment yield depends on the watershed's geologic terrain, severity of vegetation loss, and the timing of a rain event with respect to the watershed recovery process (Moody *et al.*, 2007; Ouyang *et al.*, 2010; Ryan *et al.*, 2011). Gartner *et al.* (2008) determined that slopes greater than 30% are more erodible.

Kunze and Stednick (2006) stated the quantity of bare soil plays an important role in sediment yields.

Townsend and Douglas (2000) looked at three watersheds in the tropical savanna of Northern Australia. They compared the effects of surface hydrology from three fire regimes: 1) low intensity burning early in the dry season, 2) high intensity late in the dry season, 3) and not burning. They determined that high intensity fires late in the dry season created larger areas of exposed soil. The study found degradation in the water quality of surface runoff, including high concentrations of total suspended sediments, volatile suspended sediment, phosphorus, manganese, nitrogen, and iron for the fires late in the dry season. Low intensity fires that occurred early in the dry season showed little or no effects on surface hydrology quality and quantity (Townsend and Douglas, 2000).

There is a fuzzy boundary between floods with high sediment yields and debris flows. Debris flows are highly correlated with the total rainfall of a storm (Gartner *et al.*, 2008). However, debris flows are hard to predict because they can originate from areas with minimal antecedent soil moisture (Cannon *et al.*, 2008), mass bulking of sediment laden water, and/or landslides (Friedel, 2011). Erosion and debris flows produce long term geomorphic impacts on a watershed; they carve out stream channels, and deposit debris downstream (Gartner *et al.*, 2008; Shakesby, 2005). Debris flows are dangerous; they can result in the loss of life, and the destruction of property (Gartner *et al.*, 2008; Cannon *et al.*, 2008).

2.2 The Roles of GIS and Remote Sensing

For scientific investigation of the fire impacts to surface hydrology, Geographic Information Systems (GIS) and remote sensing datasets are essential. According to Alemaw and Chaoka (2003), with the advancement of computing power and GIS methods, physical-based hydrologic modeling has become increasingly important in hydrology. GIS enables the exploration of physical factors that affect rainfall runoff response in watersheds and their spatial relationships. GIS accounts for the geometry of the physical properties of the input data, including geology, soil type, LCLU (land cover/land use), topography, unevenly distributed precipitation, and other weather information. These data are useful for spatial representation of the physical components of a watershed for visualization (Shen *et al.*, 2013) and computation of quantitative hydrology modeling. GIS offers graphic and quantitative analysis tools that are used to process geospatial data (Al-Sabhan *et al.*, 2003).

The accuracy of input variables is important for the hydrologic model to correctly represent physical processes. Spatial resolution and data accuracy are important factors in GIS data computation and hydrology model performance. For example, a Digital Elevation Model (DEM) is used to delineate the watershed, identify flow paths, slope, and flow direction. The locations of the hydro features computed from a DEM depend on the spatial resolution of the DEM (Shen *et al.*, 2013). This implies that using DEMs with different spatial resolutions can produce different model output results.

Remotely sensed imagery has proven to be very useful for LCLU classification used for analyzing the effects of LCLU change in a watershed (Nie *et al.*, 2011; Jat, 2009). Remotely sensed data is often the primary resource available for studies that

examine short and long-term LCLU change. Nie *et al.* (2011) derived LCLU information from 1973-1997 Landsat data to assess the hydrologic response as a result of land cover change in a watershed. They used four LCLU inputs from four time periods to simulate the hydrologic components in order to quantify change in hydrology for their watershed.

Multispectral imagery is useful for the classification of impervious and vegetation cover at the pixel level. Vegetated and impermeable surfaces have different effects on surface hydrology with respect to their roles in hydrologic processes, such as infiltration, evapotranspiration, etc. In general, vegetated areas have a lower curve number (CN) than impermeable surfaces. A higher curve number represents higher potential for surface runoff generation. Therefore, accurate classification of both vegetation and impermeable surfaces in a watershed are important. Reistetter and Russell (2011) used high-spatial resolution land-cover, imperviousness, and tree canopy density data to enhance surface runoff estimation by using the CN runoff method (Natural Resources Conservation Services, 1986). They concluded that the use of remote sensing imagery facilitates accurate modeling of rainfall-runoff response by modifying the Natural Resources Conservation Services (NRCS) discrete CN classes into composite CNs, because imagery provides current information about urban land cover (Reistetter and Russell, 2011).

Ouyang *et al.* (2010) used the MODIS sensor to calculate monthly and annual NDVI (Normalized Difference Vegetation Index) values in order to assess the relationship between vegetation, sediment transport, and erosion for a three-year time period. Kinoshita and Hogue (2011) used MODIS to calculate the Enhanced Vegetation Index (EVI) to look at the long term post-fire vegetation recovery and resilience in two watersheds. They stated that NDVI is useful for assessing fire damage immediately after

a fire, but that EVI was better suited for long-term vegetation recovery. EVI is less sensitive to atmosphere and soil interference than NDVI (Kinoshita and Hogue, 2011).

2.3 The Soil and Water Assessment Tool (SWAT) Model

A common model to be coupled with GIS and remote sensing in hydrologic application is the SWAT model, which is an open-source continuous-event, semi-distributed, physical model for watershed-scale analyses. The model was developed to assess the impact of land management and land use on water, sediment, and agriculture chemical yields (Arnold *et al.*, 2012, Gassman *et al.*, 2007). The SWAT model has been implemented for a variety of watershed studies around the world. Arnold *et al.* (2011) reviewed SWAT model use, calibration, and validation. According to Arnold *et al.* (2011), applications using the SWAT model have looked at the hydrology of a watershed (Lee *et al.*, 2011; Abbaspour *et al.*, 2007), sediment (Ouyang *et al.*, 2010), snowmelt, irrigation, brush removal, land use impacts (Lee *et al.*, 2011; Nie *et al.*, 2011), pollution loss studies, climate change impact studies (Moradkhani *et al.*, 2010), bacteria life cycle and transport, best management practice (BMP) scenarios (Pisinaras *et al.*, 2010), and the influence of karst features in a watershed. The SWAT model has been integrated with other types of models to do, for example, environmental, ecological, and economic assessments (Arnold *et al.*, 2011). The SWAT model requires high amount of input parameters which complicates model parameterization and calibration (Arnold *et al.*, 2011). Additionally, physical processes are subject to over simplification (Arnold *et al.*, 2011).

Arnold *et al.* (2011) states that the coefficient of determination (R^2), and Nash-Sutcliffe Efficiency (NSE) are the most commonly reported statistics used in SWAT calibration and validation. A NSE greater than 0.5 indicates a satisfactory performance of a SWAT simulation of monthly values, and that the standard can be decreased from daily values, and increased for annual values (Arnold *et al.*, 2011; Nie *et al.*, 2011), and a R^2 of 0.5 represents satisfactory performance (Nie *et al.*, 2011). NSE results greater than 0.75 represent a very good performance (Moriassi *et al.*, 2006).

Lee *et al.* (2011) studied the performance of the SWAT model's ability to quantify long-term fresh water inflows into the Gulf of Mexico. They developed two separate SWAT models to compare the Galveston Bay watershed (an urbanized watershed) and Matagorda Bay watershed (a mostly rural watershed). They used 32 years of streamflow data from 1977 to 2008. They compared the results of the SWAT model with that of the TxRR hydrology Model. Lee *et al.* (2011) stated that the SWAT model was sensitive to land cover, and land cover change over time. Urbanized areas produced the greatest differences in surface water yield between the two models. For calibration, Lee *et al.* (2011) used a streamflow data range that included the time period of the land cover data. They stated that land cover change explained why the results of the validation were not as strong as the results of the calibration.

Nie *et al.* (2011) used the SWAT model to assess changes in land use and land cover in the arid San Pedro watershed of southeastern Arizona. The North American Landscape Characterization project (i.e., LCLU information extracted from Landsat imagery) was used for land cover data for four time periods. The study used multiple regression analysis to quantify the effects of LCLU change over time on the hydrology of

the watershed. They stated that without accurate quantification of the effects of the LCLU change, the results could be under or over estimated. They determined that the growing urban areas resulted in an increase in both surface runoff and water yield. They also reported that the invasion of Mesquite on desert scrub/ grassland had resulted in a decrease in base flow and an increase in evapotranspiration.

Ouyang *et al.* (2010) investigated the relationship between vegetation cover, soil erosion, and sediment yield at different temporal-spatial scales in the upper Yellow River watershed in western China. The watershed is primarily composed of grassland and forest land; and the climate is generally cold and dry, with seasonal variability. They extracted NDVI from MODIS imagery to simulate soil erosion and transport for three years using the SWAT model. The study compared results at the basin and subbasin spatial scales, and the monthly and annual temporal scales. The study concluded that areas with higher vegetation prevented sediment transport; however, areas with higher NDVI and steep slopes contributed the most soil erosion. They determined that vegetation plays a significant role for predicting soil erosion and sediment transport for the study area, and that slope is an important factor in the production of soil erosion and sediment transport.

2.4 Summary

Wildfire can transform the hydrological dynamics of a watershed. It has been found that the level of hydrologic interruption from wildfire depends on the magnitude of a wildfire, the timing and magnitude of rain events, and the physical, climatic, and ecological characteristics of a watershed. Wildfire intensity and the physical

characteristics of a watershed govern the resilience and recovery of vegetation and therefore, the time period of the interruption.

Studies have demonstrated that GIS is a useful tool for geocomputation, and geovisualization for hydrology modeling. Additionally, remote sensing is a useful resource for LCLU data acquisition for watershed studies where timing is key to understanding the impact of LCLU on surface hydrology. This study will utilize GIS and remote sensing to investigate the impact of the 2011 Bastrop Complex Wildfire on surface hydrology.

3. METHODOLOGY

3.1 Research Questions

This research addresses the following questions:

1) Are there significant differences in simulated surface runoff between the pre- and post-Bastrop Complex Wildfire in terms of peak discharge (Q_p), time to peak (T_p) and runoff volume (R_v)?

2) Are there significant differences in simulated sediment yield (Y) between the pre- and post-Bastrop Complex Wildfire?

3.2 Study Area

The study area was determined based on the drainage area for the stream segment between the two U.S. Geological Survey (USGS) stream gages in the lower Colorado River watershed, including the Colorado River at Bastrop, TX gage (08159200) (U.S. Geological Survey, 2014a), and the Colorado River at Smithville, TX gage (08159500) (U.S. Geological Survey, 2014b) (Figure 3). The total area of the stream segment catchment (i.e., the study area) is 1,248 square kilometers (482 square miles) and the Bastrop Complex Wildfire burn scar is approximately 130 square kilometers (50 square miles) (Figures 3 and 4). The stream segment was selected for this study because the total area of the Colorado River watershed is quite large relative to the area of the burn scar. The total drainage area of the Colorado River at the outlet of the study area (i.e., the Smithville gage) is 104,560 square kilometers (40,371 square miles), and the contributing drainage area of the Colorado River basin is 75,027 square kilometers (28,968 square

miles) (U.S. Geological Survey, 2014b). The Colorado River originates in eastern New Mexico and flows south-east to Matagorda Bay and the Gulf of Mexico.

Bastrop County is located in Central Texas. According to the 2010 U.S. Census, Bastrop County had a population of 74,169 (U.S. Census Bureau, 2014). Land use in the study area primarily consists of low density residential developments, protected park land, and agriculture crop land.

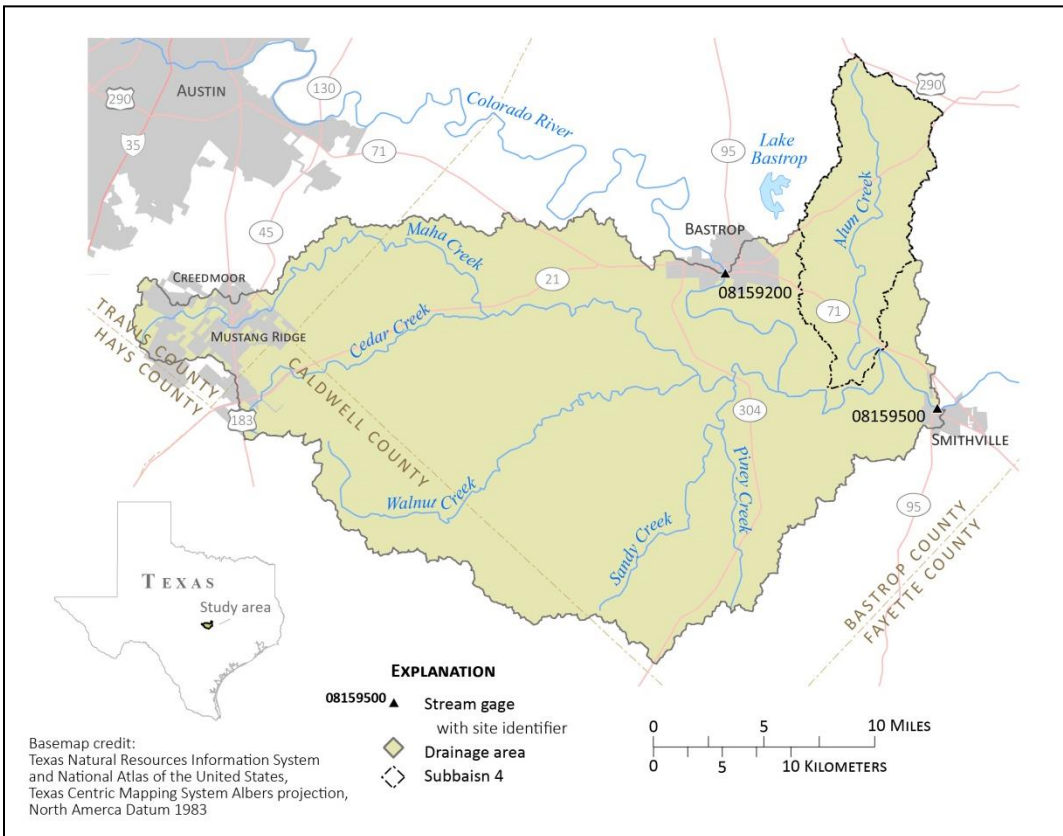


Figure 3. The study area–drainage area for the Colorado River stream segment between the USGS streamgaging-stations at Bastrop and Smithville, TX.

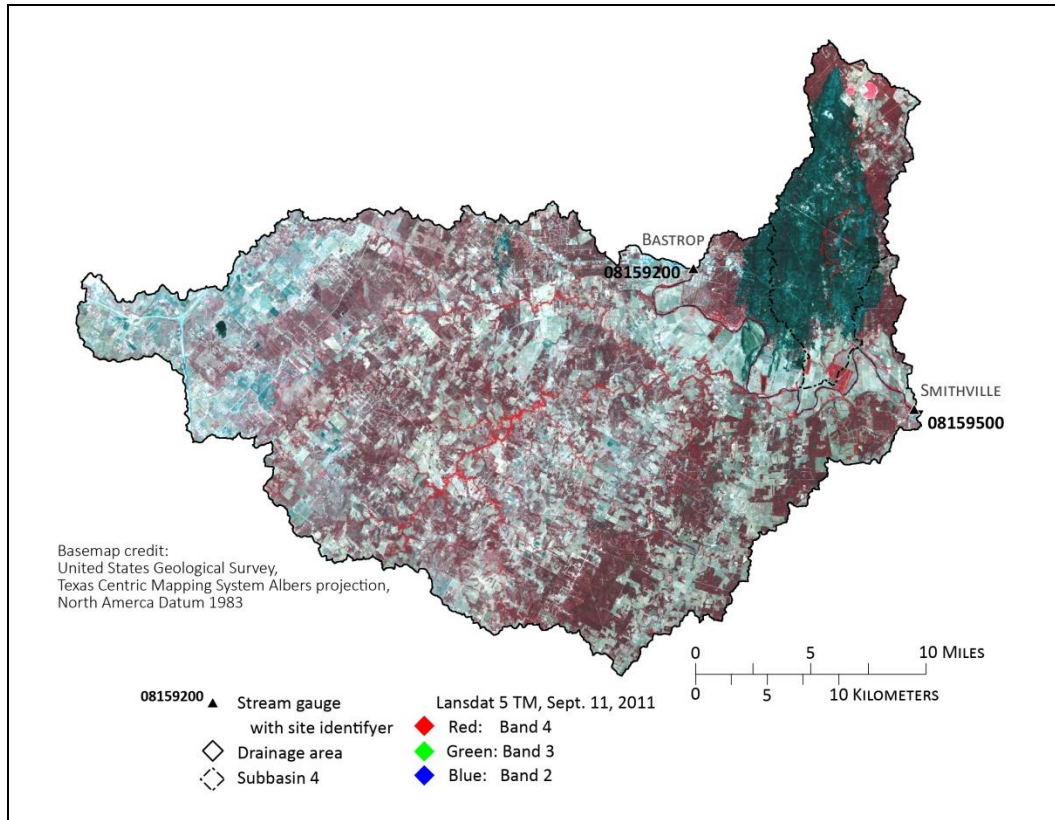


Figure 4. A Landsat 5 image (RGB432) on September 11, 2011, showing the Bastrop Complex Wildfire burn scar within the study area.

3.3 Data

Landsat 5 TM multispectral imagery was used for LCLU classification. The National Elevation Data (NED) from U.S. Geological Survey (USGS) was used for 10 meter spatial resolution digital elevation model (DEM). USGS stream gages were used for surface water quantity data (Figure 5). The National Centers for Environmental Prediction (NCEP) Climate Forecast System Reanalysis (CFSR) was used for weather data, including relative humidity, average daily solar radiation, temperature, precipitation, and daily average wind speed from 15 weather stations. The NRCS SSURGO data provided the description about the soil type. The model was trained using 21 years of

continuous daily observed streamflow data produced by the USGS Bastrop stream gage (i.e., January 1, 1990 to December 31, 2010). The Smithville gage had 13 years of observed daily values available to use for calibration and validation.

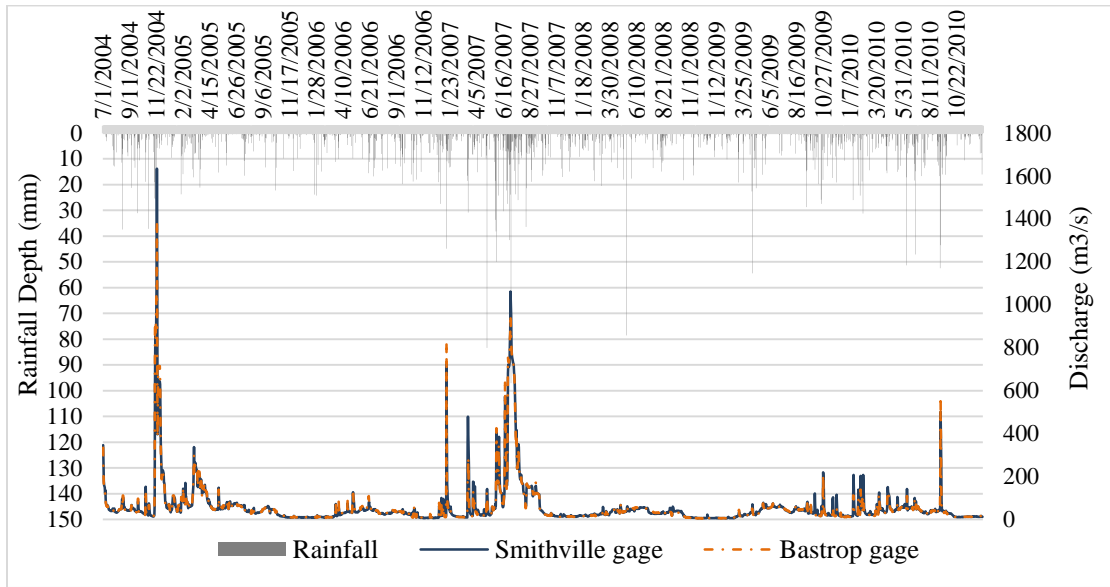


Figure 5. Observed streamflow and precipitation in the study area from July 2004 to December 2010.

3.4 SWAT Model

The SWAT surface water hydrology model was used for this study. The model uses topographic, LCLU, and soil data to determine the surface water runoff quantity for the Colorado River watershed. Moreover, sediment volume is calculated for the drainage area of the study area.

SWAT used the 10 meter DEM to delineate the drainage area between the Bastrop gage location (for upstream inflow), and Smithville gage (the pour point of drainage area). SWAT generates the flow paths of the streams within the drainage area

based on the DEM. Slope information was extracted from the DEM. SWAT automatically subdivided the study area into 21 subbasins based on stream segments of the tributaries within the study catchment area. The subbasins are further divided into 219 hydrologic response units (HRU) based on LCLU, surficial soil, and slope. The model computes hydrologic variables at the scale of the HRU.

The LCLU information was created using two Landsat 5 TM images. The pre-fire image was acquired on August, 26, 2011, and the post-fire image was acquired on October 13, 2011, after the fire was extinguished. Two SWAT models were created with the same set of data inputs and calibrated model parameters (to be explained further in following section), except for the LCLU. The LCLU changes immediately before and after the Bastrop Complex Wildfire were used to reflect the changes in the watershed landscape and simulate its impacts in post-fire surface hydrology. The Landsat 5 imagery is provided by the USGS with the standard terrain correction (NASA, 2011). The at-sensor radiometric calibration uncertainty is around 5% for Landsat 5 (Chander, 2009).

Unsupervised classification with a maximum of 40 iterations generated 140 spectral classes. The spectral classes were grouped into the nine LCLU classes used in the hydrologic model, including: evergreen and mixed forest, scrub/shrub land, open space/low density urban areas, and medium/high urban land cover, pasture, crop land, barren, water. The LCLU classes were selected based on the classes required for the Natural Resource Conservation Service (NRCS) CN method (Soil Conservation Service, 1986). The study used stratified random sampling to perform the accuracy assessment. In order to meet accuracy objectives, the number of test points used for land cover accuracy assessment was determined using the multinomial distribution method as follow:

$$N = B \Pi_i (1 - \Pi_i) / b_i^2 \quad (1)$$

where Π_i denotes the proportion of the population in the i -th class out of k classes; b_i denotes the desired precision; and B_i denotes the upper percentile of Chi-square distribution. The test points were compared with National Agriculture Imagery Program (NAIP) aerial imagery and Google Earth for validation. Accuracy assessment of the LCLU classification was summarized in a confusion matrix in order to compute the classification accuracy and Kappa analysis. The Kappa Coefficient of Agreement statistic is computed as:

$$\hat{K} = \frac{N \sum_{i=1}^r x_{ii} - \sum_{i=1}^r (x_{i+} * x_{+i})}{N^2 - \sum_{i=1}^r (x_{i+} * x_{+i})} \quad (2)$$

where N denotes the total number of observations; r denotes the number of land cover classes; x_{ii} denotes the marginal totals of row i and column i ; x_{i+} denotes the total for column i ; and x_{+i} denotes the total for row i . Overall accuracy was calculated using the confusion matrix accuracy:

$$\text{Overall accuracy} = x/n \quad (3)$$

where x denotes the number of test points that have been correctly classified, and n denotes the total number of test points used to compare observed data to land cover classification data.

The simulated results are produced by the hydrologic balance equations. The model simulated a total of 21 years: a 5 year warm up period was used, resulting in 16 years of simulated output values. The surface hydrology simulation uses the NRCS Curve Number (CN) model to calculate surface runoff:

$$I = 0.2S$$

$$S = (1000/CN) - 10$$

$$Q_{surf} = \frac{(R_{day} - I_a)^2}{(R_{day} - I_a + S)} \quad (4)$$

where Q denotes runoff quantity (mm H₂O); R is rainfall; I denotes abstraction (interception, infiltration) (mm H₂O); and S denotes soil moisture retention (mm H₂O).

CNs are generated based on the non-linear relationship of soil absorptive capacity, which depends on soil type and land cover type. The modified rational method is used to predict peak runoff:

$$Q_{peak} = C * i * Area / 3.6 \quad (5)$$

where Q_{peak} denotes peak runoff rate (m³/s); C is runoff coefficient; $Area$ denotes area of the watershed (km²); and i denotes interception (mm/hr). Manning's roughness coefficient is used to calculate velocity:

$$v_{ov} = \frac{q_{ov}^{0.4} \cdot slp^{0.3}}{n^{0.6}} \quad (6)$$

where v denotes velocity (m/s); q_{ov} denotes over land flow (m^3/s); slp denotes Slope (m/m); n denotes Manning's roughness coefficient. The model uses the Modified Universal Soil Loss Equation (MUSLE) to simulate sediment yield:

$$sed = 11.8 \cdot (Q_{surf} \cdot q_{peak} \cdot area_{hru})^{0.56} \cdot K_{USLE} \cdot C_{USLE} \cdot P_{USLE} \cdot LS_{USLE} \cdot CFRG \quad (7)$$

where sed denotes sediment yield (metric tons); Q_{surf} denotes Surface water runoff volume ($mm \text{ H}_2\text{O/ha}$); Q_{peak} denotes peak runoff rate (m^3/s); $Area$ denotes area of HRU (ha); K_{usle} denotes soil erodability factor; C_{usle} denotes cover and management factor; LS_{usle} denotes topographic factor; and $CFRG$ denotes course fragment factor.

3.4.1 Calibration

Calibration is used to identify and adjust model parameters in order to improve water yield simulation performance. A variety of options are available for calibration and validation of SWAT model results. Manual calibration was used for this project. Manual calibration gives the user the ability to fine tune model parameters based on physical knowledge of the watershed. Observed values from the USGS Colorado River at Smithville gage were divided into two subsets of data. The USGS gage provided 13 years of continuous daily observed values that were suitable for this project, therefore the calibration and validation data sets are both 6.5 years in duration. Both data sets include a balanced representation of dry, average, and wet streamflow conditions. A stream record

that is representative of the possible streamflow conditions (i.e., low, high, and average) is recommended for SWAT calibration, and it is important for a central Texas watershed where extreme climate variability is regularly experienced. The model was calibrated with the data set that is temporally consistent with the data inputs used in the model (e.g., 2004-2010). Sediment yield is simulated but not calibrated for this study, because there is no sediment yield observation data produced at the Smithville gaging station.

The simulation results were compared to the observed streamflow to calculate the model performance. Objective functions are used to assess the predictive abilities of the SWAT simulation. The Nash-Sutcliffe Efficiency (NSE) and the Coefficient of Determination (R^2) are the most commonly reported objective functions used for the SWAT model (Arnold *et al.*, 2012). The NSE value typically ranges from one (i.e., a perfect match) to negative infinity (i.e., mismatch). In general, simulation results with a NSE value greater than 0.5 are deemed acceptable. Nash-Sutcliffe Efficiency is as follows:

$$E = 1 - \frac{\sum_{t=1}^T (Q_o^t - Q_m^t)^2}{\sum_{t=1}^T (Q_o^t - \overline{Q_o})^2} \quad (8)$$

where Q_o denotes observed discharge and Q_m denotes simulated discharge (Moriassi, 2006). The Coefficient of Determination is an indicator of how well a model will predict a phenomenon; for example if R^2 is 0.7, then the simulated data explains 70 percent of the variation in the observed data. The Coefficient of Determination is calculated as follows:

$$R^2 \equiv 1 - \frac{SS_{err}}{SS_{tot}}. \quad (9)$$

where SS_{err} denotes the sum of the squares of residuals, and SS_{tot} denotes the sum of the squares.

Multiple parameters were adjusted during manual calibration: Base-flow (ALPHA_BF); hydraulic conductivity (CH_K2); water movement from shallow aquifer to root zone (GW_REVAP); and available water capacity (SOL_AWC). The calibrated simulation uses data that was collected before the Bastrop Complex Wildfire and therefore is known as the “pre-fire” simulation. In order to generate the post-fire scenario, the post-fire LCLU data was applied to the calibrated pre-fire model to produce the “post-fire” simulation.

Table 1. Calibration and validation objective function results.

Analysis Period	NSE	R ²
Pre-fire calibration period	0.94	0.95
Pre-fire validation period	0.83	0.83

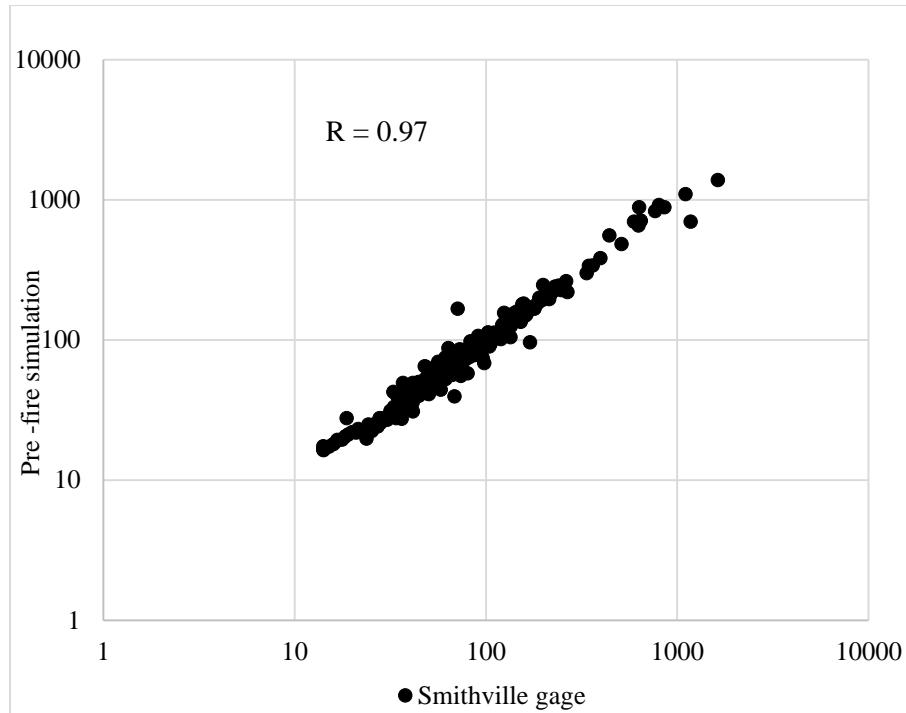


Figure 6. Scatter plot diagram comparing observed to simulated daily streamflow values.

3.4.2 Statistical Analysis

The data flow diagram (Figure 7) describes the procedure that was applied before the wildfire (T1) and after the wildfire (T2). The results of the simulations were compared to explore changes in the surface hydrology. Two geographic extents were examined: the study area, and the subbasin that experienced the greatest damage from the fire. Three temporal scales are used to statistically examine the null hypotheses between the pre- and post-fire hydrology: continuous, multimodal, and unimodal. The continuous daily values simulation was separated into the calibration and validation periods in order to explore surface runoff, and sediment yield. A series of rain events resulting in a multimodal, and unimodal rainfall-runoff response events generated from 30 mm (1.2 in),

50 mm (2 in), 80 mm (3.1 in) rain events were extracted from the continuous simulation to look at surface runoff, sediment yield, peak discharge, and time to peak. The duration of the discrete events starts before the rise in the hydrograph and ends after the drop in the hydrograph; therefore the duration of the hydrographs vary. In order to accept or reject the null hypothesis, paired *t*-test and the Wilcoxon test (i.e., when the hydrologic responses are not normally distributed) were used to quantify statistical differences in the pre- and post-fire simulations at the 0.05 level. Peak discharge and time to peak were qualitatively examined using the discrete event hydrographs.

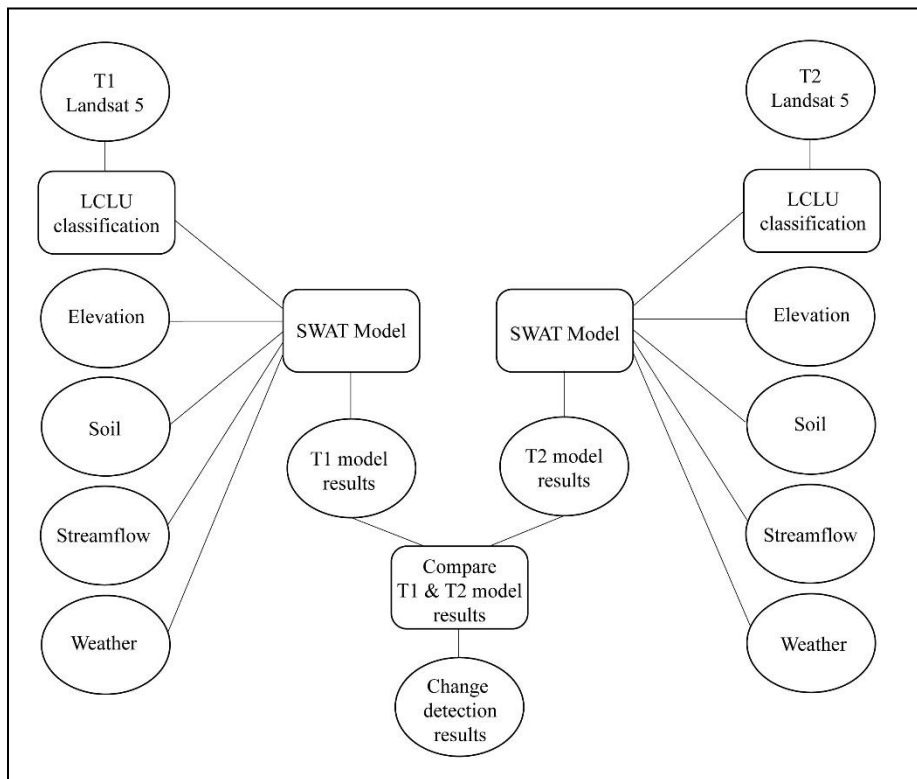


Figure 7: Data-flow Diagram.

4. RESULTS

4.1 LCLU Classification

Two Landsat 5 images were used for pre- and post-fire land cover classification. The multinomial distribution method was applied to the images to determine the number of test points needed for accuracy with a 95% probability and a 10% precision. The multinomial distribution method resulted in 17 test points for the October 13, 2011 image and 18 test points for the August, 26, 2011 image. The test points were used to compare the land cover classification with National Agriculture Imagery Program (NAIP) aerial imagery, and Google Earth for validation. The August classification resulted in an overall accuracy of 0.61 (Table 4), and a Kappa value of 0.56. The October classification produced an overall accuracy of 0.72 (Table 5), and a Kappa value of 0.68. Both Kappa values represent good agreement between observed and predicted LCLU class assignment. The barren land cover in the study area changed from 0.05 square kilometers to 109.32 square kilometers (Table 2). Subbasin 4 resulted in a 65.07 square kilometers increase in barren land cover (Table 3).

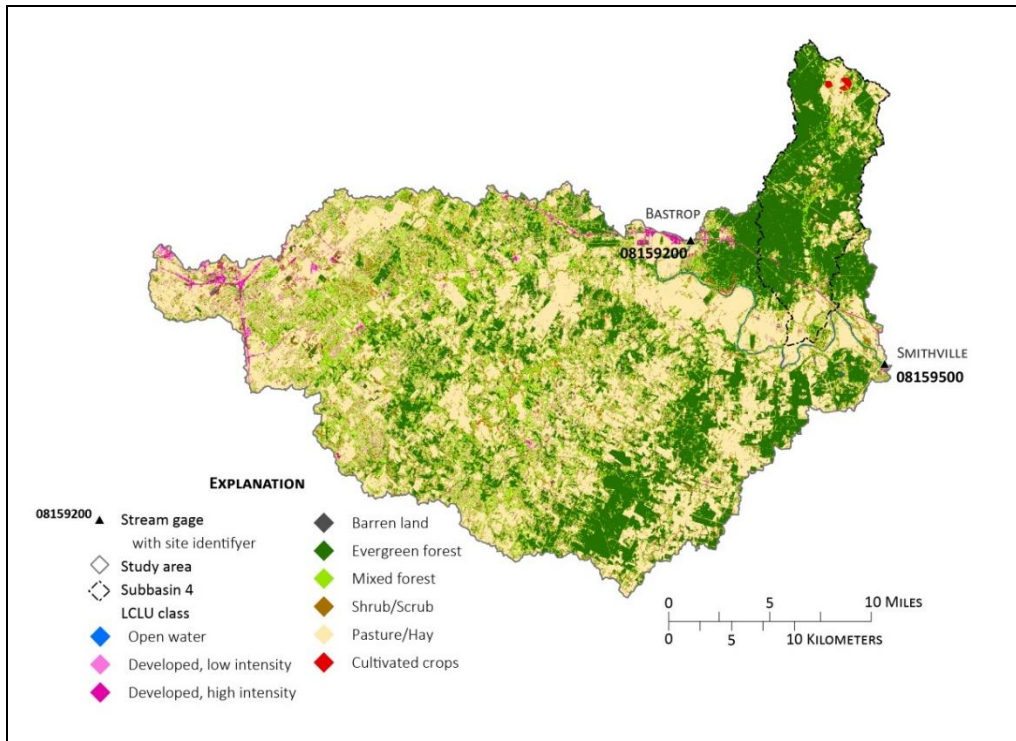


Figure 8. August pre-fire LCLU classification.

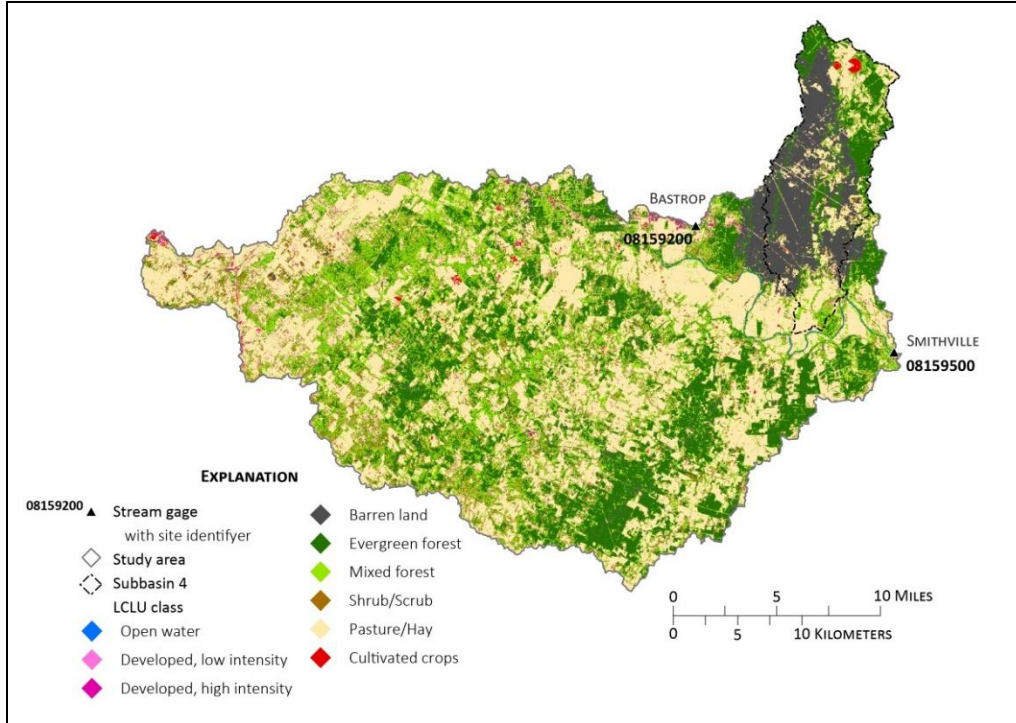


Figure 9. October post-fire LCLU classification.

Table 2. LCLU change from August and October 2011 for the study area.

LCLU Class	August LCLU Area, km ²	August LCLU %	October LCLU Area, km ²	October LCLU %	LCLU change
Open Water	2.94	0%	2.15	0%	-27%
Developed, Low Intensity	78.36	6%	38.64	3%	-51%
Developed, Medium Intensity	12.98	1%	10.50	1%	-19%
Barren Land (Rock/Sand/Clay)	0.05	0%	109.32	9%	211,355%
Evergreen Forest	351.52	28%	349.82	28%	0%
Mixed Forest	255.57	20%	242.07	19%	-5%
Shrub/Scrub	79.90	6%	89.34	7%	12%
Pasture/Hay	459.75	37%	399.97	32%	-13%
Cultivated Crops	7.35	1%	6.62	1%	-10%

Table 3. LCLU change from August and October 2011 for subbasin 4.

LCLU Class	August LCLU Area, km ²	August LCLU %	October LCLU Area, km ²	October LCLU %	LCLU change
Open Water	0.05	0.0%	0.03	0%	-43%
Developed, Low Intensity	3.00	2.1%	1.24	1%	-59%
Developed, Medium Intensity	0.57	0.4%	1.77	1%	210%
Barren Land (Rock/Sand/Clay)	0.00	0.0%	65.07	46%	n/a
Evergreen Forest	89.66	63.0%	31.09	22%	-65%
Mixed Forest	16.02	11.3%	10.85	8%	-32%
Shrub/Scrub	5.36	3.8%	5.42	4%	1%
Pasture/Hay	26.13	18.4%	25.50	18%	-2%
Cultivated Crops	1.44	1.0%	1.24	1%	-13%

Table 4. LCLU classification error matrix for August 2011.

Class	Open Water	Developed, Low Intensity	Developed, Medium Intensity	Barren Land	Evergreen Forest	Mixed Forest	Shrub/Scrub	Pasture/Hay	Cultivated Crops	Row total
Open Water	18		1							19
Developed, Low Intensity		5				1	1	1	3	11
Developed, Medium Intensity			11	9						20
Barren Land		1	2	7						10
Evergreen Forest					14					14
Mixed Forest					3	16	1		5	25
Shrub/Scrub		7		1	1		12	3	8	32
Pasture/Hay		5	4	1		1	4	14		29
Cultivated Crops									2	2
Column Total	18	18	18	18	18	18	18	18	18	162
Overall accuracy:	99 / 162 = 61%									

Table 5. LCLU classification error matrix for October 2011.

Class	Open Water	Developed, Low Intensity	Developed, Medium Intensity	Barren Land	Evergreen Forest	Mixed Forest	Shrub/Scrub	Pasture/Hay	Cultivated Crops	Row total
Open Water	17		1							
Developed, Low Intensity		7	3	1		2		1	6	20
Developed, Medium Intensity			10						1	11
Barren Land		1	3	14						18
Evergreen Forest					15					15
Mixed Forest		4		2	2	12	1			21
Shrub/Scrub		5				2	13	2		22
Pasture/Hay						1	3	14	2	20
Cultivated Crops									8	8
Column Total	17	17	17	17	17	17	17	17	17	153
Overall accuracy:	110 / 153 = 72%									

4.2 SWAT Model

The SWAT model continuous record simulation results were separated into two analyses: (1) the simulation of the study area (i.e. the drainage area between Bastrop and Smithville gages within the lower Colorado River watershed), and (2) the simulation for the subbasin that experience to most damage from the wildfire (i.e., subbasin 4). Discrete rain events were extracted from the three periods to compare the pre- and post-wildfire SWAT simulation of surface water yield and sediment yield.

Observed inflow data at the Bastrop gage was used for the simulation. The SWAT model was calibrated and validated by comparing simulated pre-fire streamflow to observed streamflow at the Smithville gage downstream. There was no observed sediment data available for inflow or outflow, therefore the results of the sediment yield were not calibrated.

In order to focus the examination of wildfire impacts on surface hydrology, the subbasin that experienced the most damage from the wildfire (i.e., subbasin 4) was used in addition to the study area. Subbasin 4 was one of the 21 subbasins delineated by SWAT. Unfortunately, observed streamflow data at the outlet of subbasin 4 was not available as there is no existing stream gage at that location. As such, the subbasin 4 simulation was not calibrated; the pre- and post-fire simulations were merely compared.

The SWAT model simulated continuous streamflow for the calibration (July 2004- December 2010) and validation period (January 1998- June 2004). To better understand the wildfire impacts in surface hydrology, discrete rain event hydrographs with varying magnitude of actual rainfall events, including 30 mm (1.2 in), 50 mm (2 in), 80 mm (3.1 in) were extracted from the continuous simulation. Depending on the normality of streamflow data, either the t-test or the Wilcoxon test was used to examine

any statistically significant difference between observed and simulated streamflow. The t-test was applied to discrete rain events with normally distributed hydrographs. The Wilcoxon test was applied to hydrographs that did not have a normally distributed hydrograph (e.g., the series of multiple rain events).

4.2.1 Continuous simulation of the study area

The calibration period included continuous streamflow data from July 1, 2004 to December 31, 2010. The pre-fire calibration time period produced a NSE of 0.94, and a R^2 value of 0.95 (Table 1). The objective functions (i.e., NSE and R^2) represent very good overall simulations for the calibration period (Moriassi, 2006). For the calibration period (i.e., July 2004- December 2010), there was a 0.3% difference ($395 \text{ m}^3/\text{s}$) in pre- and post-fire surface water yield. The Wilcoxon test resulted in a significant Z score of -11.28 ($p < 0.001$). Sediment yield produced a 193% difference (69,740 metric tons), with the Wilcoxon test resulted in a significant Z score of -10.35 ($p < 0.001$).

The validation period includes continuous streamflow data from January 1, 1998 to June 30, 2004. The pre-fire validation period produced a NSE of 0.83, and a R^2 value of 0.83 (Table 1). Both objective functions represent a very good overall simulation for the validation period. (Moriassi, 2006). For the validation period, there was a 12% difference ($16,938 \text{ m}^3/\text{s}$), and the Wilcoxon test produced a significant Z score of -41.34 ($p < 0.001$) for surface water yield, rejecting the null hypothesis. Pre- and post-fire sediment yield produced an 86% difference (445,785 metric tons), and the Wilcoxon test produced a significant Z score of -10.19 ($p < 0.001$). The null hypothesis was again rejected.

4.2.2 Discrete events extracted from the continuous simulation of the study area

The calibration period pre- and post-fire simulation for the 31 mm (1.22. in) rain event produced a 0.82% change (2.73 m³/s) in surface water yield where the paired t-test produced a t score of 1.04 ($p = 0.34$) (Figure 10a). Sediment yield resulted in a difference of 660.6 metric tons, and the paired t-test resulted in $t = 1$ ($p = 0.36$) (Figure 10b). The validation period pre- and post-fire simulation for the 27 mm (1.06 in) rain event produced a 45% difference (74.26 m³/s) in pre- and post-fire surface water yield with a paired t-test result of $t = 2.27$ ($p = 0.06$) (Figure 11a). Sediment yield resulted in a 355% difference (4,548 metric tons), and the t-test produced a $t = 1$ (p value of 0.36) (Figure 11b). Hence, there were no significant differences between the pre- and post-fire surface water and sediment yield in the discrete 1-in rainfall events.

Table 6. Study area simulation totals for pre- and post-fire peak rainfall intensity, time to peak (T_p), peak discharge (Q_p), runoff volume, and sediment volume for the 30 mm (1.2 in) rain event.

Figure	Date of Event	Peak Rainfall Intensity	Simulation	Q_p , m ³ /s	T_p , days	Mean Runoff Volume, m ³ /s	Total Sediment Yield, Metric Tons
10a, 10b	09/29/2004	31 mm (1.22 in)	Pre-fire	48.14	2	328.76	0
			Post-fire	50.78	2	331.49	660.6
11a, 11b	02/21/2004	27 mm (1.06 in)	Pre-fire	28.69	2	166.73	1,280
			Post-fire	66.61	1	240.99	5,828

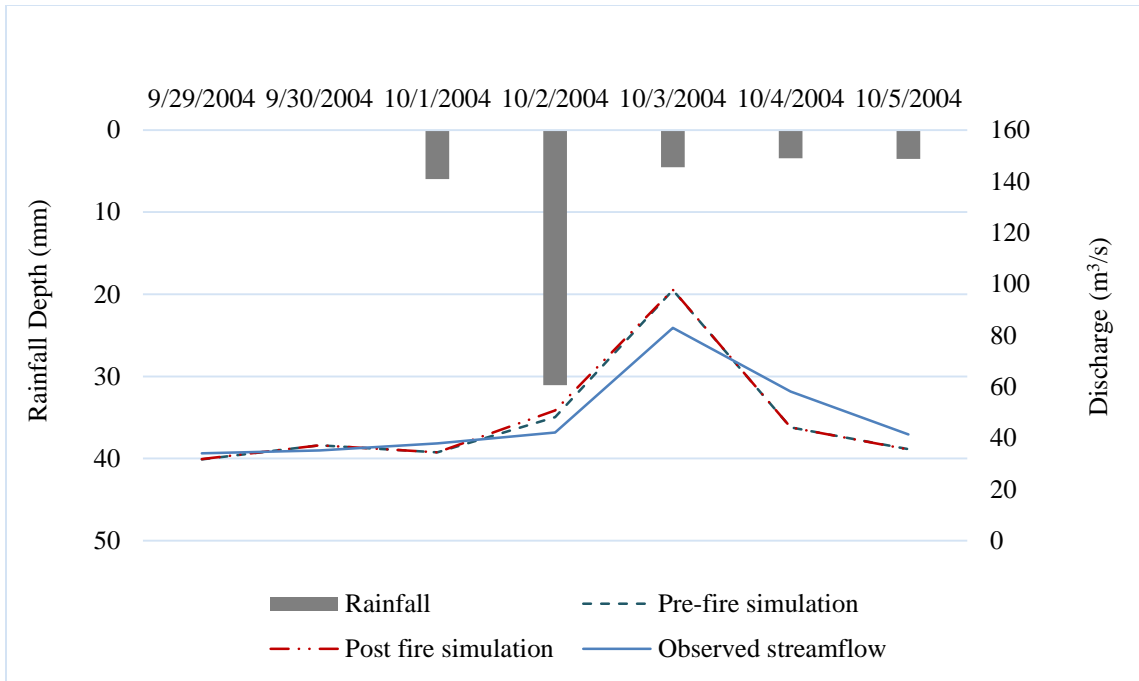


Figure 10a. Water yield generated by a 31 mm (1.22 in) rain event for the calibration period.

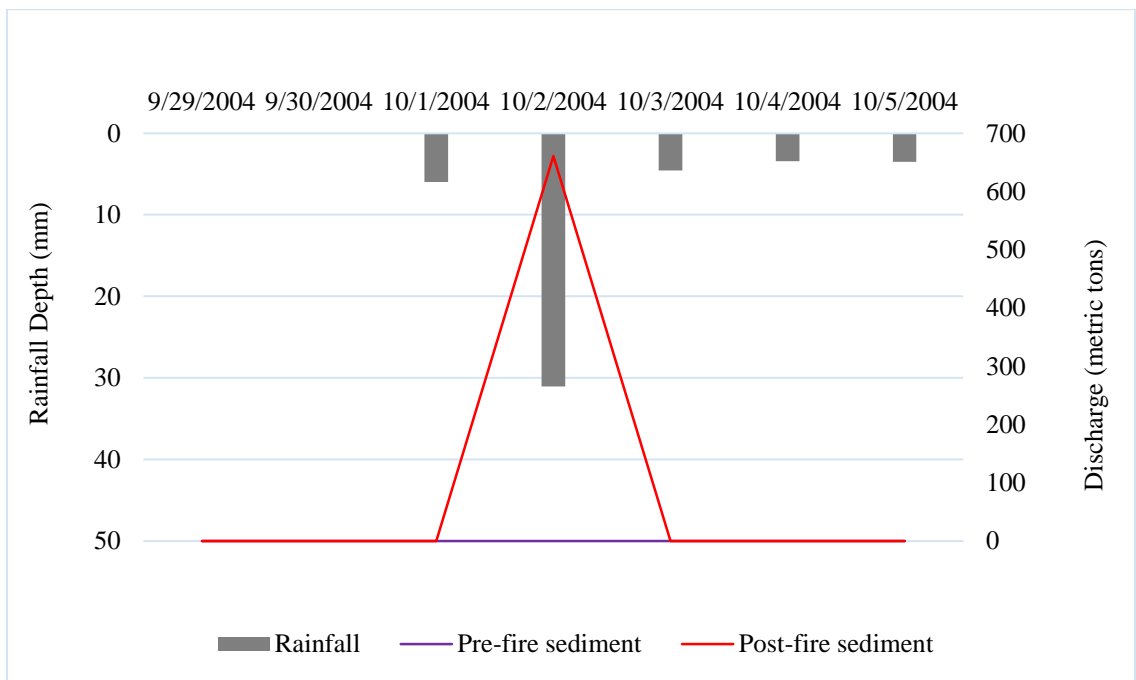


Figure 10b. Sediment yield generated by a 31 mm (1.22 in) rain event for the calibration period.

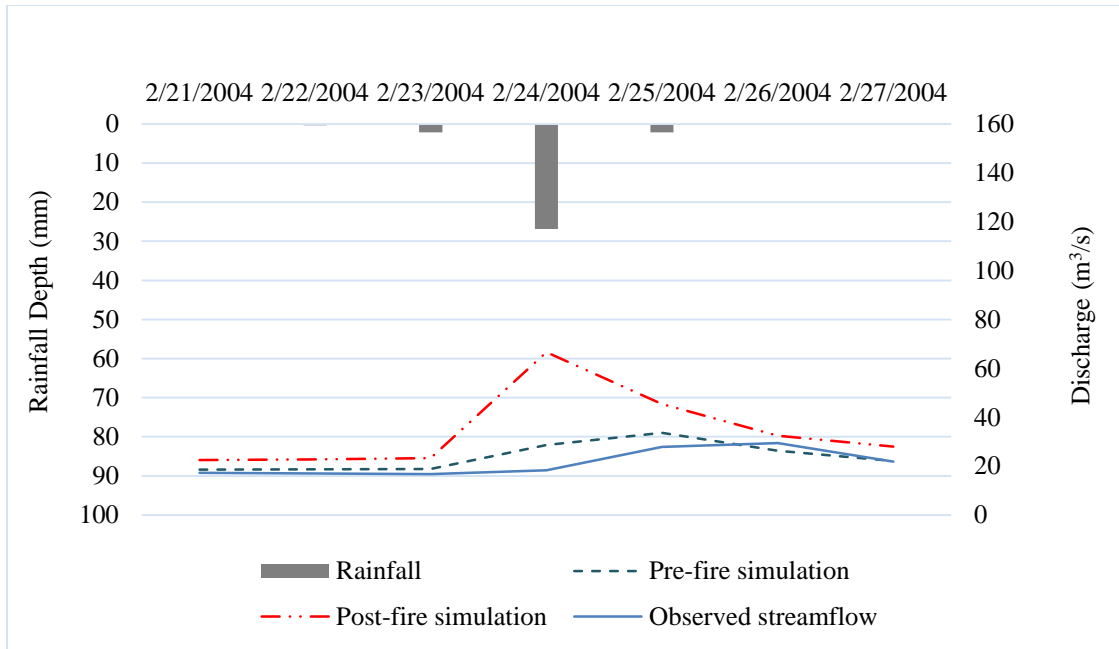


Figure 11a. Water yield generated by a 27 mm (1.06 in) rain event for the validation period.

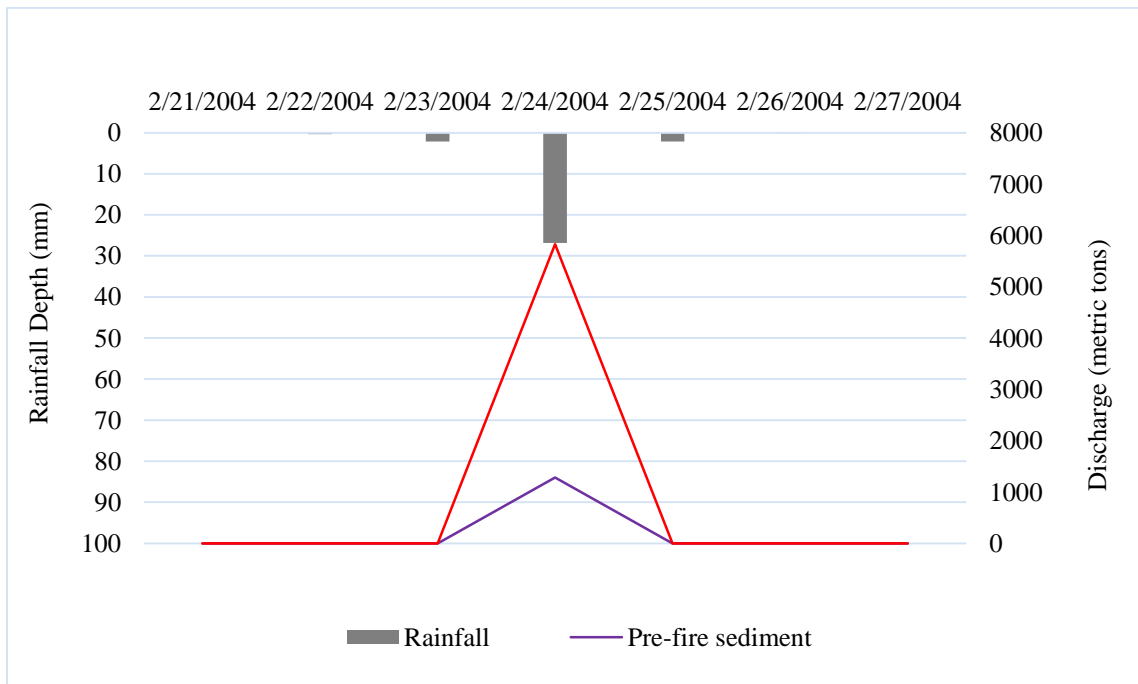


Figure 11b. Sediment yield generated by a 27 mm (1.06 in) rain event for the validation period.

The calibration period pre- and post-fire simulation for the 55 mm (2.15 in) rain event produced a 0.3% difference (0.97 m³/s) in pre- and post-fire surface water yield where the paired t-test resulted in $t = 0.5$ ($p = 0.62$) (Figure 12a). Sediment yield resulted in a 313% difference (826.83 metric tons), and a t-test of $t = 1.03$ ($p = 0.33$) (Figure 12b). The validation period pre- and post-fire simulation for the 51 mm (2.01 in) rain event produced a 61% difference (129.42 m³/s) in pre- and post-fire surface water yield with a t-test of $t = 2.11$ ($p = 0.09$) (Figure 13a). Sediment yield resulted in a 318% difference (6,293 metric tons) and a t-test of $t = 1$ ($p = 0.36$) (Figure 13b). In summary, all null hypotheses associated with the pre- and post-fire difference in surface water and sediment yield of discrete 2-in rainfall events are rejected.

Table 7. Study area simulation totals for pre- and post-fire peak rainfall intensity, time to peak (T_p), peak discharge (Q_p), runoff volume, and sediment volume for the 50 mm (2 in) rain event.

Figure	Date of Event	Peak Rainfall Intensity	Simulation	Q_p , m ³ /s	T_p , days	Mean Runoff Volume, m ³ /s	Total Sediment Yield, Metric Tons
12a, 12b	4/14/2009	55 mm (2.15 in)	Pre-fire	69.31	1	323.05	263.8
			Post-fire	71.13	1	324.02	1,090.63
13a, 13b	04/09/2004	51 mm (2.01 in)	Pre-fire	65.29	1	213.42	1,980
			Post-fire	137.6	1	342.84	8,273

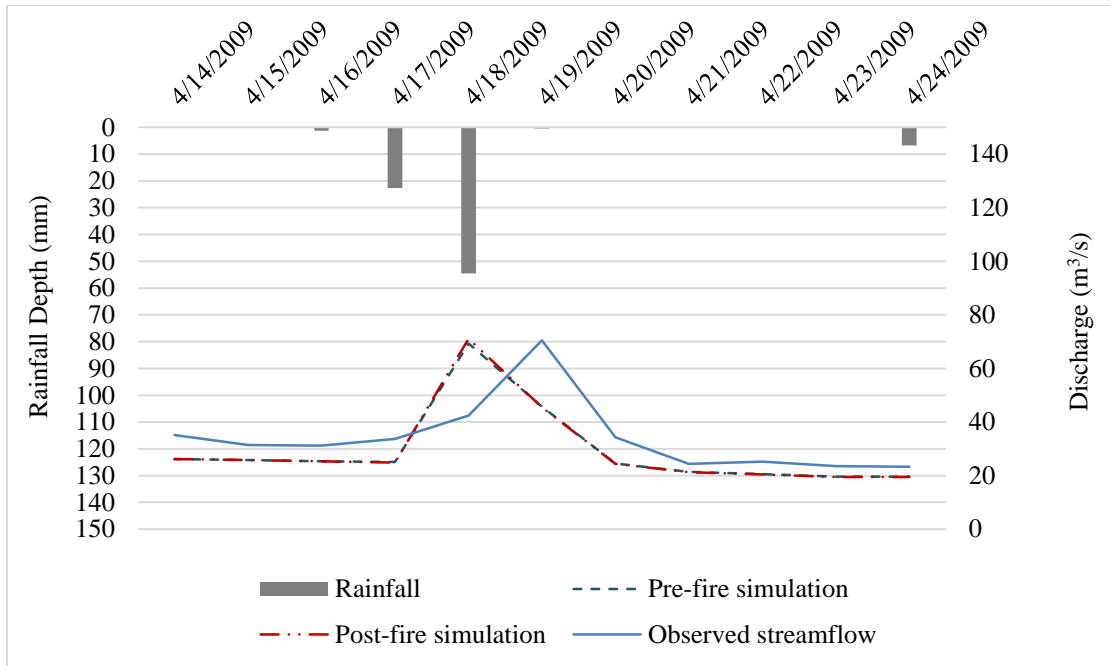


Figure 12a. Water yield generated by a 55 mm (2.15 in) rain event for the calibration period.

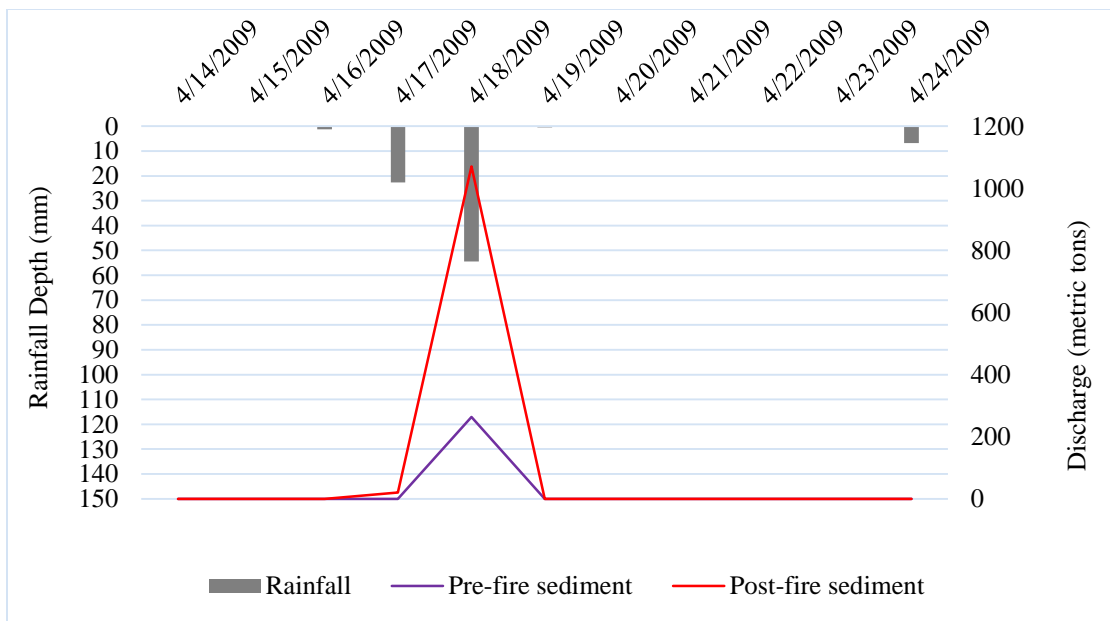


Figure 12b. Sediment yield generated by a 55 mm (2.15 in) rain event for the calibration period.

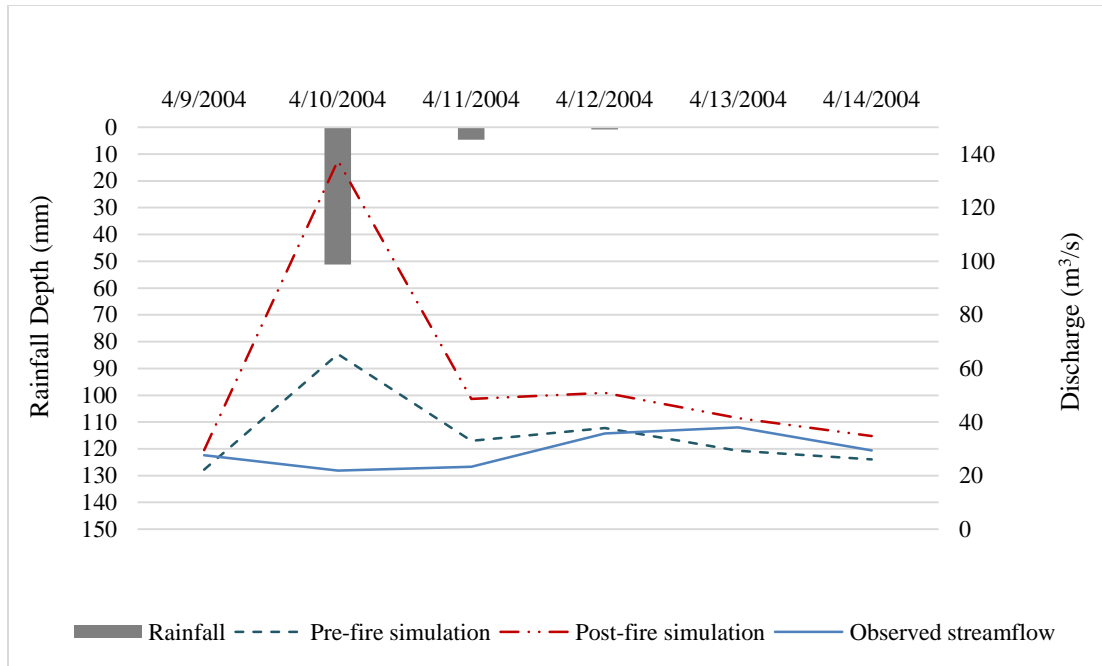


Figure 13a. Water yield generated by a 51 mm (2.01 in) rain event for the validation period.

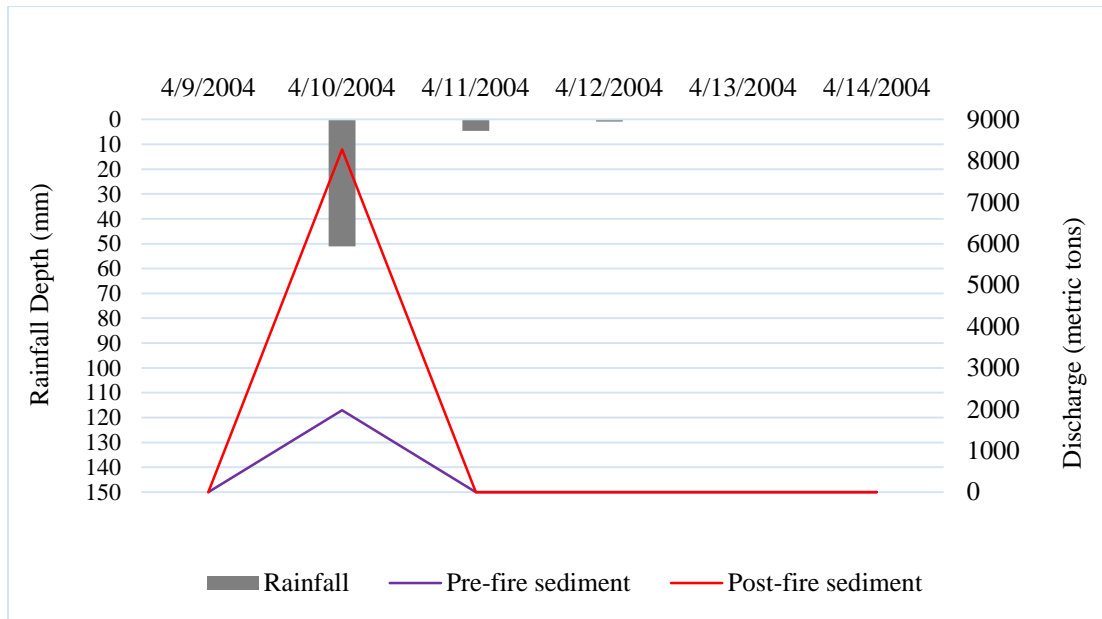


Figure 13b. Sediment yield generated by a 51 mm (2.01 in) rain event for the validation period.

The calibration period pre- and post-fire simulation for the 83 mm (3.29 in) rain event produced a 3% difference (16.73 m³/s) in pre- and post-fire surface water yield with a paired t-test where $t = 1.04$ ($p = 0.34$) (Figure 14a). Sediment yield resulted in a 269% difference (7,550 metric tons) and a t-test of $t = 1$ ($p = 0.36$) (Figure 14b). The validation period pre- and post-fire simulation for the 76 mm (3 in) rain event produced a 46% difference (279.58 m³/s) in pre- and post-fire surface water yield with a t-test of $t = 1.56$ ($p = 0.17$) (Figure 15a). Sediment yield resulted in a 1,220% difference (18,394.72 metric tons) and a t-test of $t = 1$ ($p = 0.35$) (Figure 15b). Similar to the unimodal rainfall events which did not have significant difference between pre- and post-fire hydrologic response.

Table 8. Study area simulation totals for pre- and post-fire peak rainfall intensity, time to peak (T_p), peak discharge (Q_p), runoff volume, and sediment volume for the 80 mm (3 in) rain event.

Figure	Date of Event	Peak Rainfall Intensity	Simulation	Q_p , m ³ /s	T_p , days	Mean Runoff Volume, m ³ /s	Total Sediment Yield, Metric Tons
14a, 14b	5/1/2007	83 mm (3.29 in)	Pre-fire	241	1	619.64	2,810
			Post-fire	258.8	1	636.37	10,360
15a, 15b	10/04/1998	76 mm (3 in)	Pre-fire	272.5	1	608.33	1,508
			Post-fire	465.3	1	887.91	19,902.72

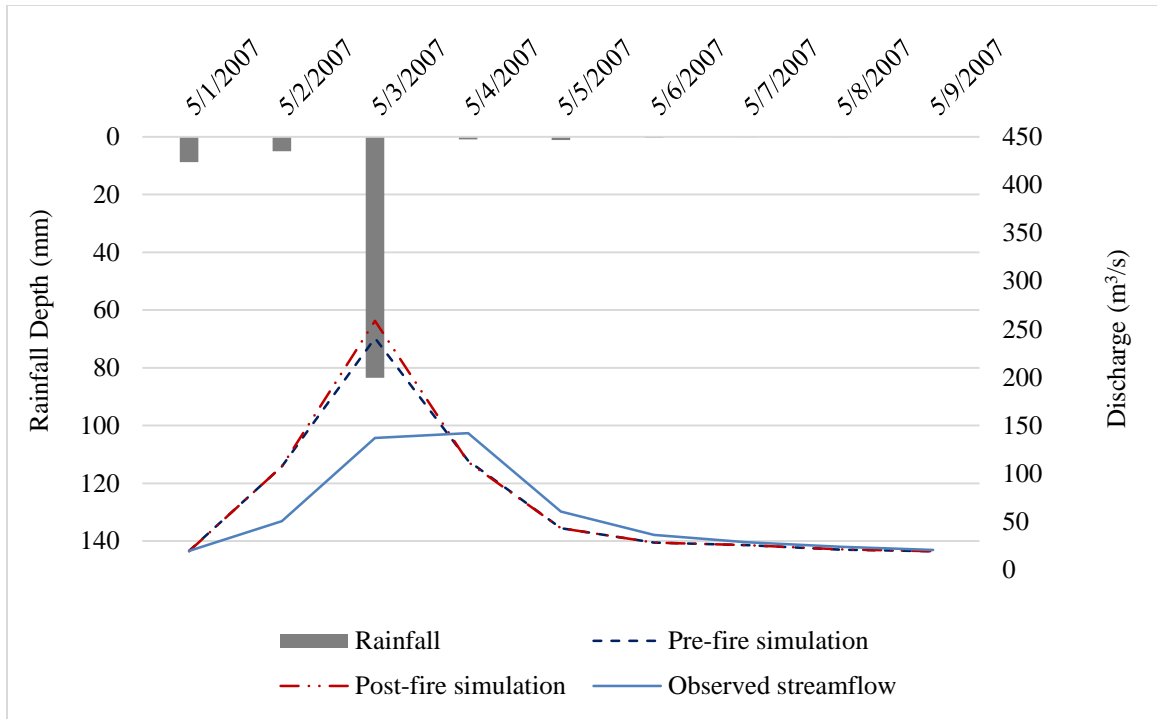


Figure 14a. Water yield generated by an 83 mm (3.29 in) rain event for the calibration period.

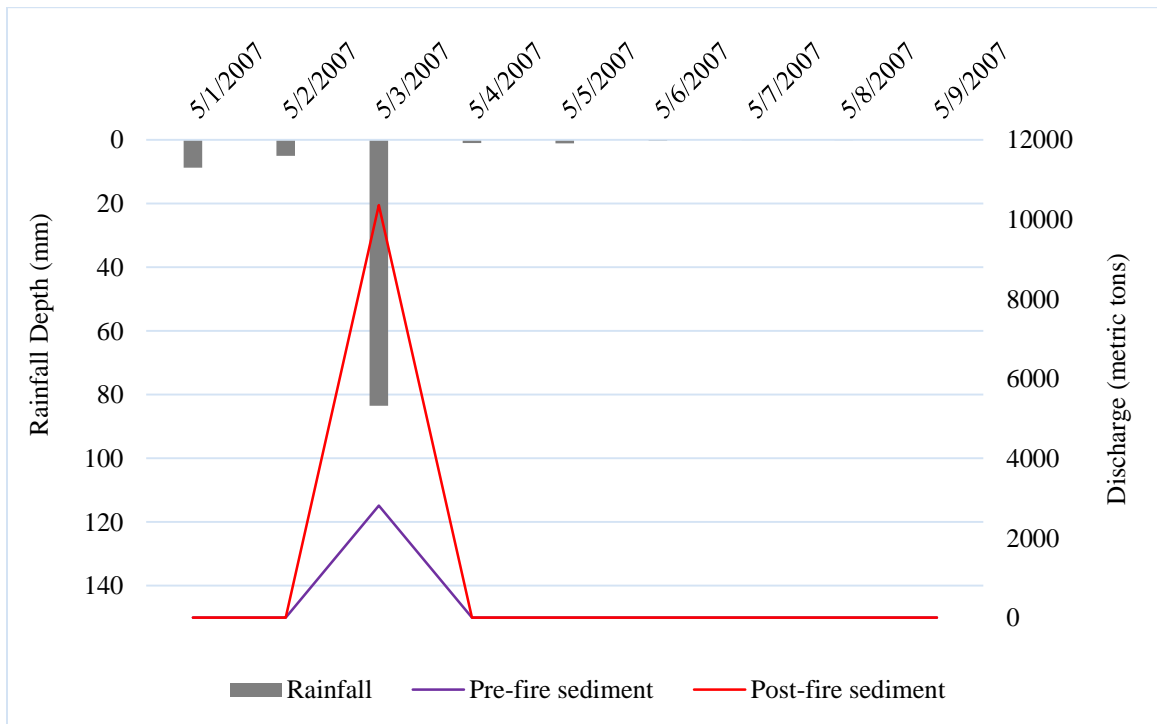


Figure 14b. Sediment yield generated by an 83 mm (3.29 in) rain event for the calibration period.

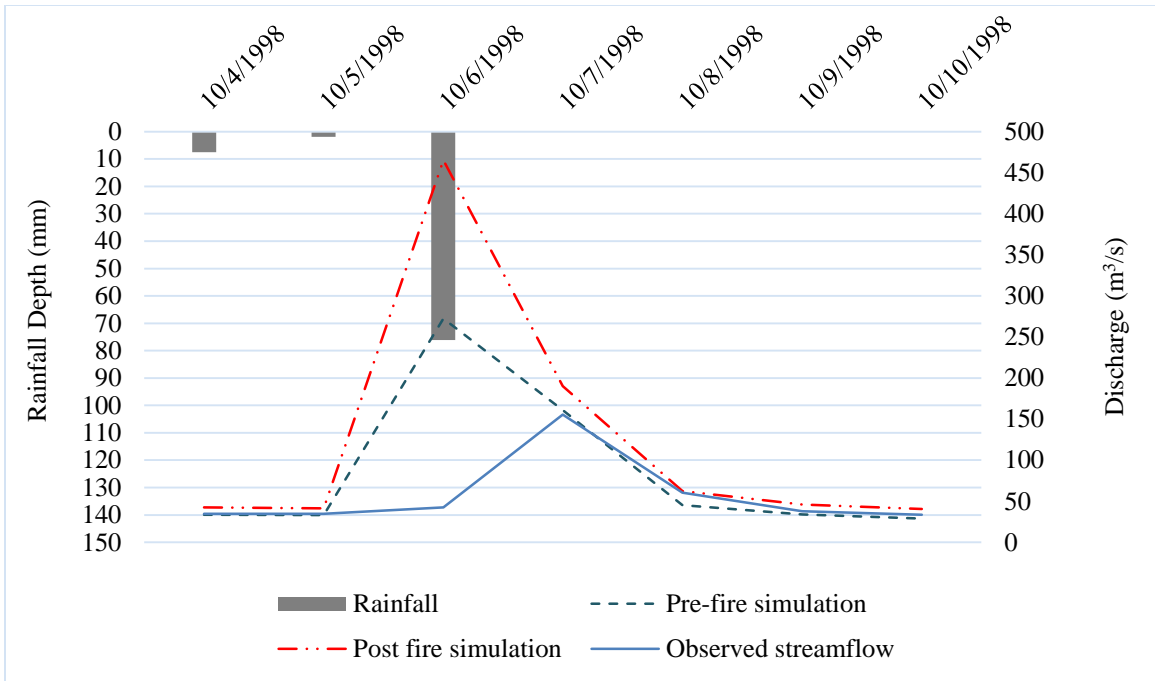


Figure 15a. Water yield generated by a 76 mm (3 in) rain event for the validation period.

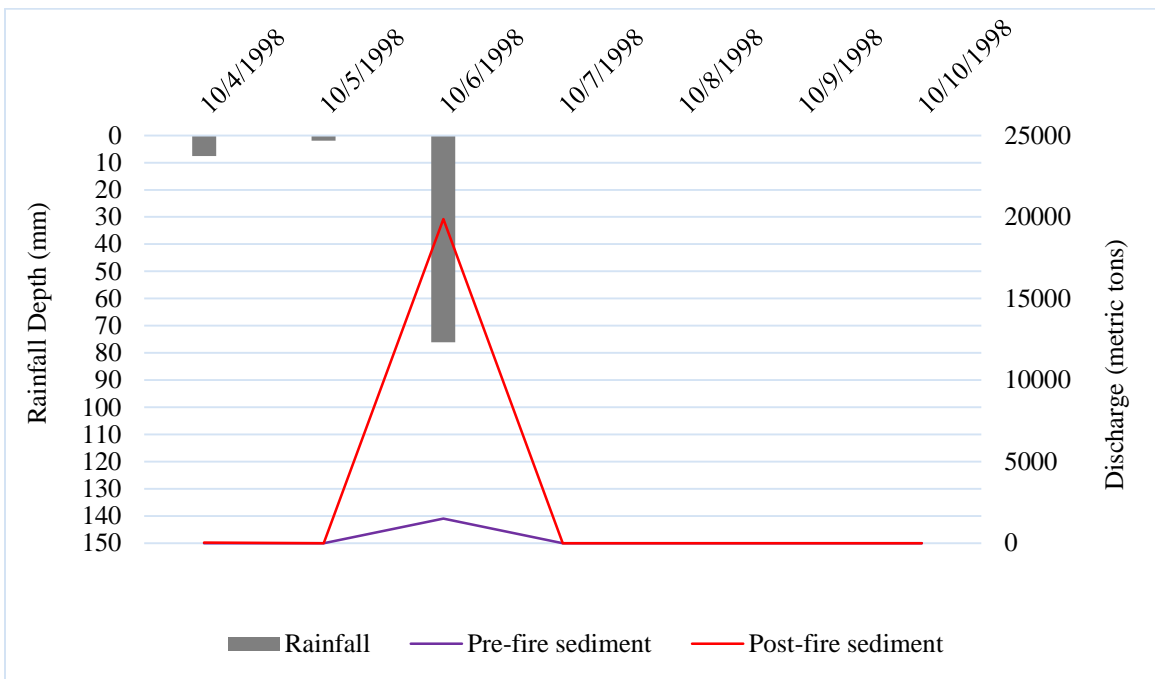


Figure 15b. Sediment yield generated by a 76 mm (3 in) rain event for the validation period.

The calibrated simulation for the multimodal event with rainfall peaks in 25 mm (1 in), 26 mm (1.01 in), and 42 mm (1.66 in) produced a 21% difference (2,876.8 m³/s) in pre- and post-fire surface water yield (Figure 16a), and the Wilcoxon test for surface water resulted in a significant Z score of -4.20 ($p < 0.001$). Post-fire sediment yield increased by 6,270% (8,873.2 metric tons) (Figure 16b), and the Wilcoxon test resulted in a significant Z score of -2.37 ($p < 0.02$). Similarly, the validation period pre- and post-fire simulation for the 32 mm (1.25 in), 13 mm (0.5 in), 13 mm (0.52 in) rain events produced an 1% difference (38.85 m³/s) in pre- and post-fire surface water yield (Figure 17a), and the Wilcoxon test produced a significant Z score of -5.91 ($p < 0.001$). Sediment yield resulted in a 315% difference (5,186.69 metric tons) (Figure 17b), and the Wilcoxon test produced a significant Z score of -2.10 ($p = 0.04$). All null hypotheses of the multimodal events were rejected.

Table 9. Study area simulation totals for pre- and post-fire peak rainfall intensity, time to peak (T_p), peak discharge (Q_p), runoff volume, and sediment volume for the series of rain events.

Figure	Date of Event	Peak Rainfall Intensity	Simulation	Q_p , m ³ /s	T_p , days	Mean Runoff Volume, m ³ /s	Total Sediment Yield, Metric Tons
16a, 16b	11/14/2004	42 mm (1.66 in)	Pre-fire	1,386	2	13,477.55	141.52
			Post-fire	1,387	2	16,354.35	9,014.72
17a, 17b	01/27/98	32 mm (1.25 in)	Pre-fire	168.4	2	3,679.5	1,648.44
			Post-fire	169.4	2	3,718.35	6,835.14

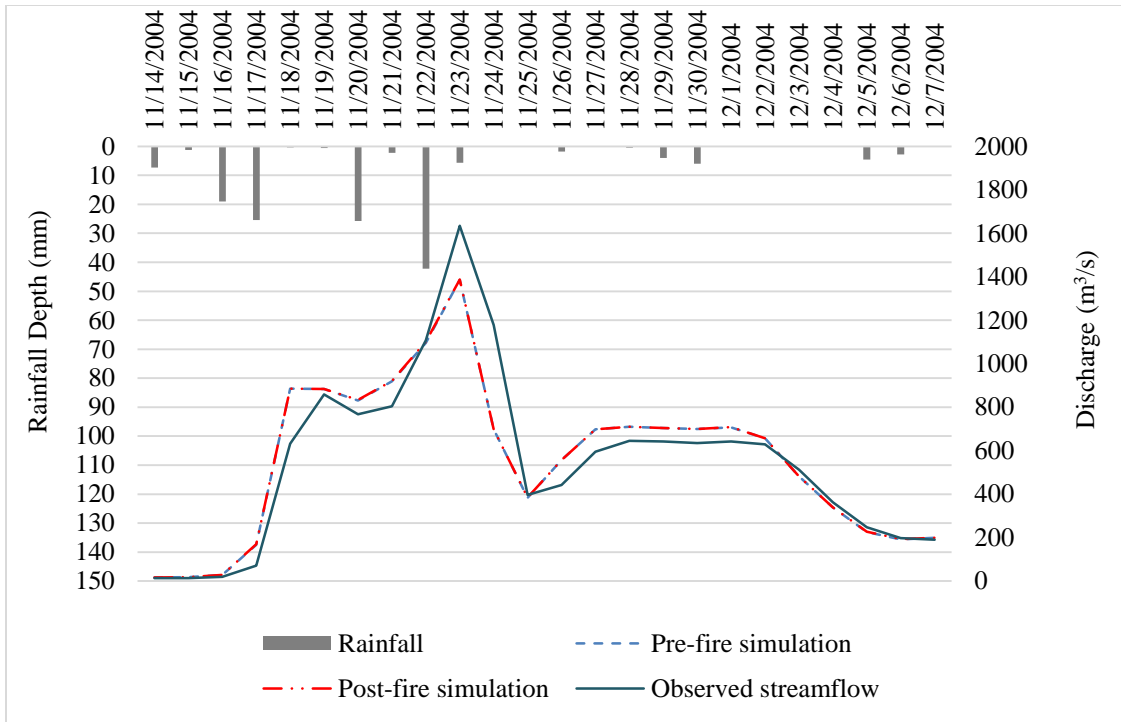


Figure 16a. Water yield generated by 25 mm (1 in), 26 (1.01 in), and 42 (1.66 in) rain events for the calibration period.

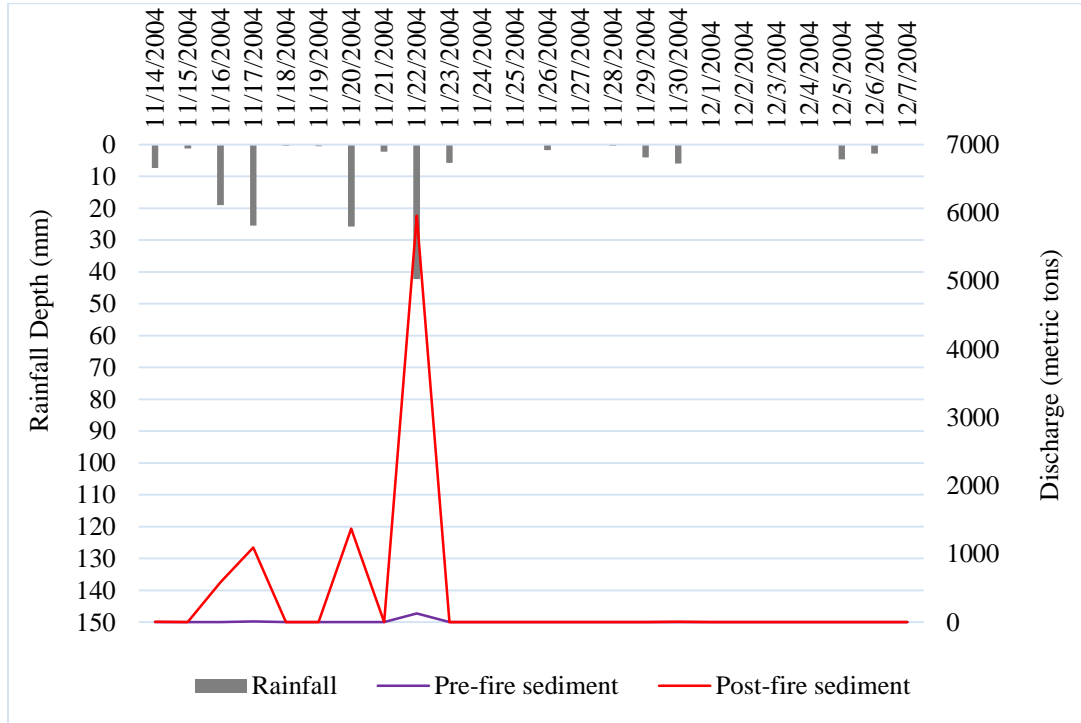


Figure 16b. Sediment yield generated by 25 mm (1 in), 26 (1.01 in), and 42 (1.66 in) rain events for the calibration period.

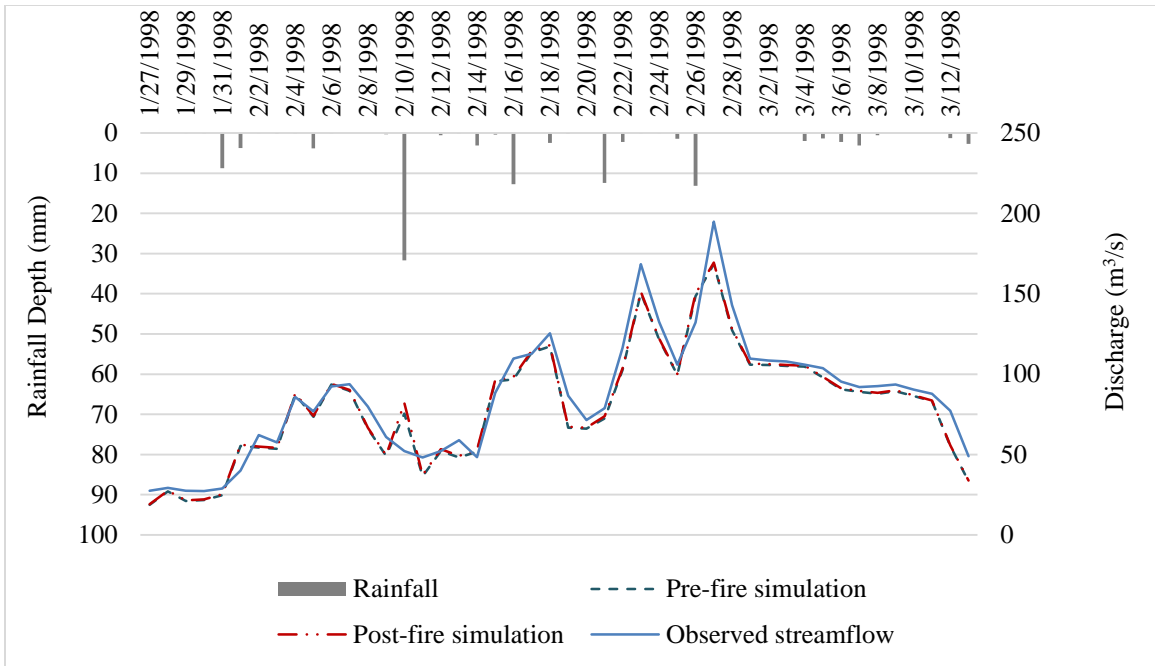


Figure 17a. Water yield generated by 32 mm (1.25 in), 13 mm (0.5 in), 13 mm (0.52 in) rain events for the validation period.

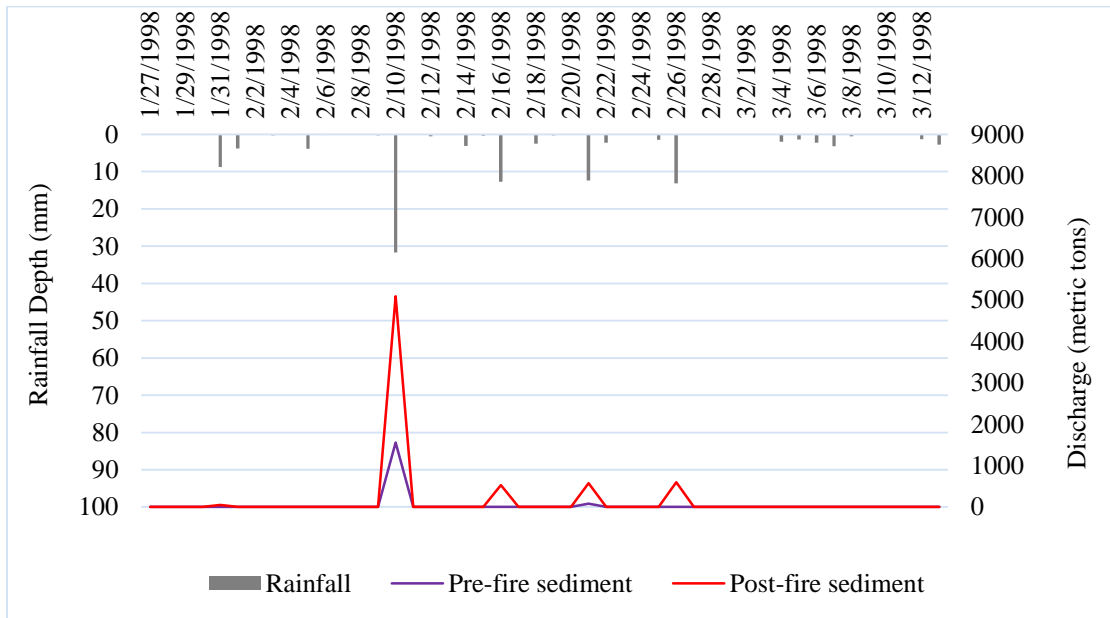


Figure 17b. Sediment yield generated by 32 mm (1.25 in), 13 mm (0.5 in), 13 mm (0.52 in) rain events for the validation period.

4.2.3 Simulation at Subbasin 4

The calibration period includes continuous pre- and post-fire streamflow data from July 1, 2004 to December 31, 2010. For the calibration period, there was a 107% difference (809.94 m³/s) surface water yield, and the Wilcoxon test resulted in a significant Z value of -36.33 ($p > 0.001$). Post-fire sediment yield increased by 8,041% (74,386 metric tons), the Wilcoxon test again resulted in a significant Z value of -33.29 ($p > 0.001$).

The pre- and post-fire simulation for the discrete 31 mm (1.22 in) rain event produced a 289% difference (6.8 m³/s) in pre- and post-fire surface water yield with a t -score of 1.76 ($p = 0.13$) (Figure 18a). Sediment yield resulted in a 480,000,000,000% difference (660 metric tons), and a t-test resulted in a $t = 1$ ($p = 0.36$) (Figure 18b). The p values failed to reject the null hypotheses.

Table 10. Subbasin 4 simulation totals for pre- and post-fire peak rainfall intensity, time to peak (T_p), peak discharge (Q_p), runoff volume, and sediment volume for the 31 mm (1.22 in) rain event.

Figure	Date of Event	Peak Rainfall Intensity	Simulation	Q_p , m ³ /s	T_p , days	Mean Runoff Volume, m ³ /s	Total Sediment Yield, Metric Tons
18a, 18b	09/29/2004	31 mm (1.22 in)	Pre-fire	0.63	1	2.34	1.83*10 ⁻⁷
			Post-fire	4.79	1	9.11	659.91

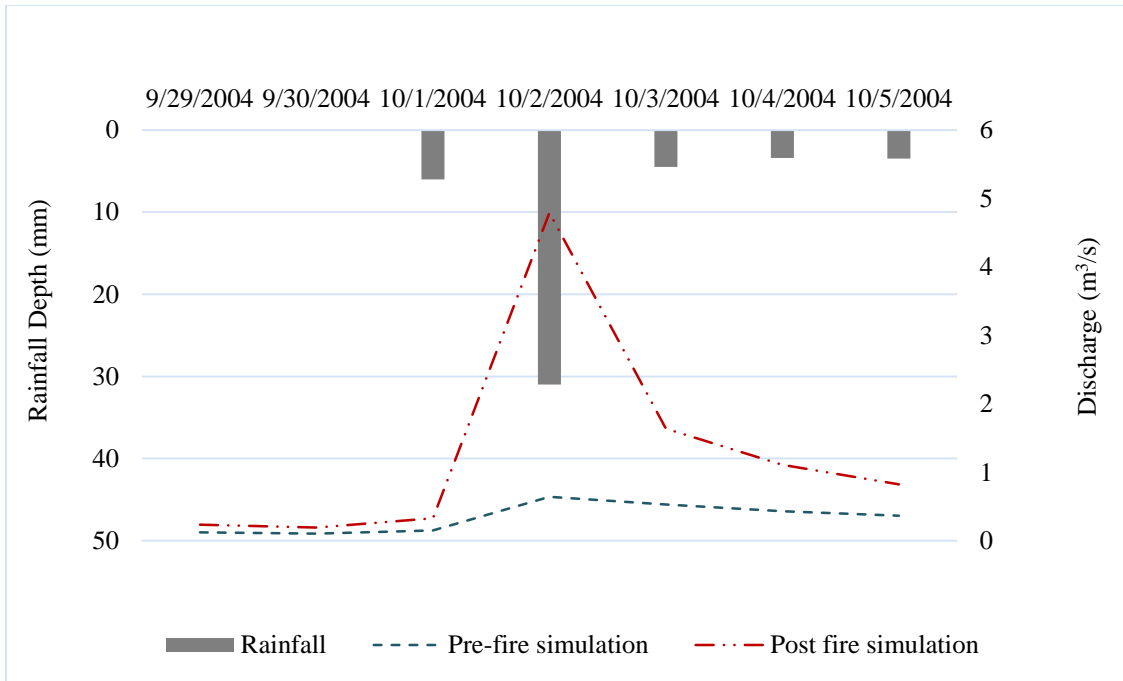


Figure 18a. Water yield generated by a 31 mm (1.22 in) rain event for the calibration period.

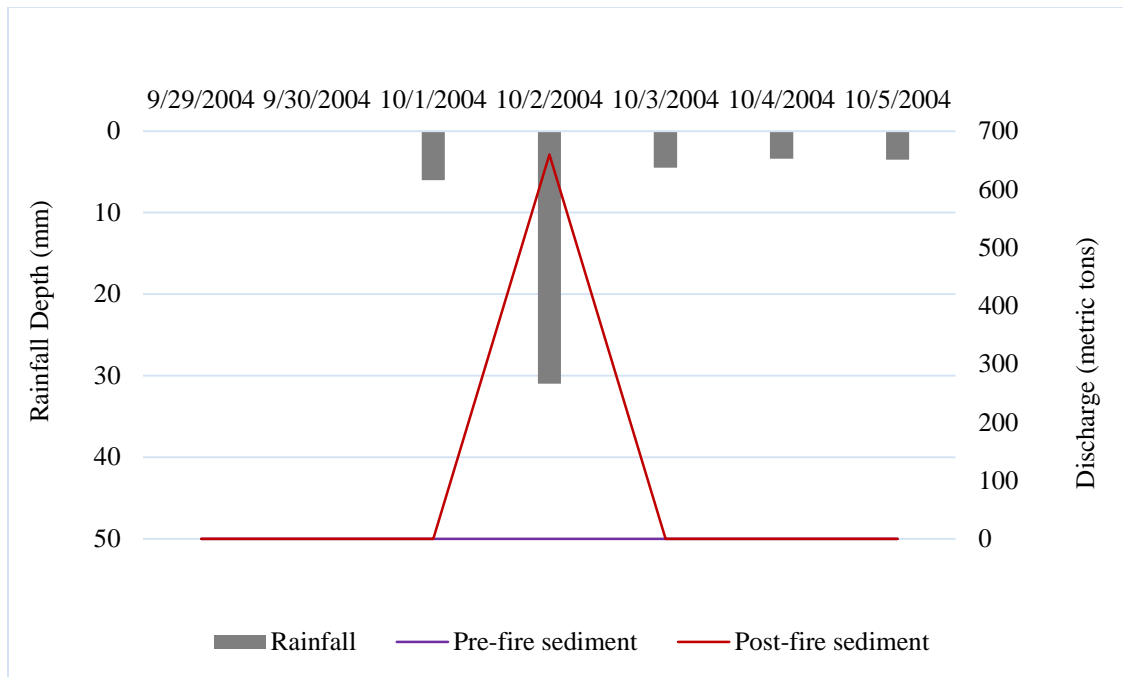


Figure 18b. Sediment yield generated by a 31 mm (1.22 in) rain event for the calibration period.

The pre- and post-fire simulation for the discrete 55 mm (2.15 in) rain event produced a 183% difference (11.7 m³/s) in pre- and post-fire surface water yield with a t-test of $t = 1.9$ ($p = 0.09$) (Figure 19a). Sediment yield resulted in a 14,082% difference (871.87 metric tons) and a t-test of $t = 1.03$ ($p = 0.33$) (Figure 19b). The null hypotheses of pre- and post-fire difference in surface water and sediment yield associated with this discrete event were rejected.

Table 11. Subbasin 4 simulation totals for pre- and post-fire peak rainfall intensity, time to peak (T_p), peak discharge (Q_p), runoff volume, and sediment volume for the 55 mm (2.15 in) rain event.

Figure	Date of Event	Peak Rainfall Intensity	Simulation	Q_p , m ³ /s	T_p , days	Mean Runoff Volume, m ³ /s	Total Sediment Yield, Metric Tons
19a, 19b	04/14/2009	55 mm (2.15 in)	Pre-fire	2.55	1	6.39	6.19
			Post-fire	8.91	1	18.11	877.37

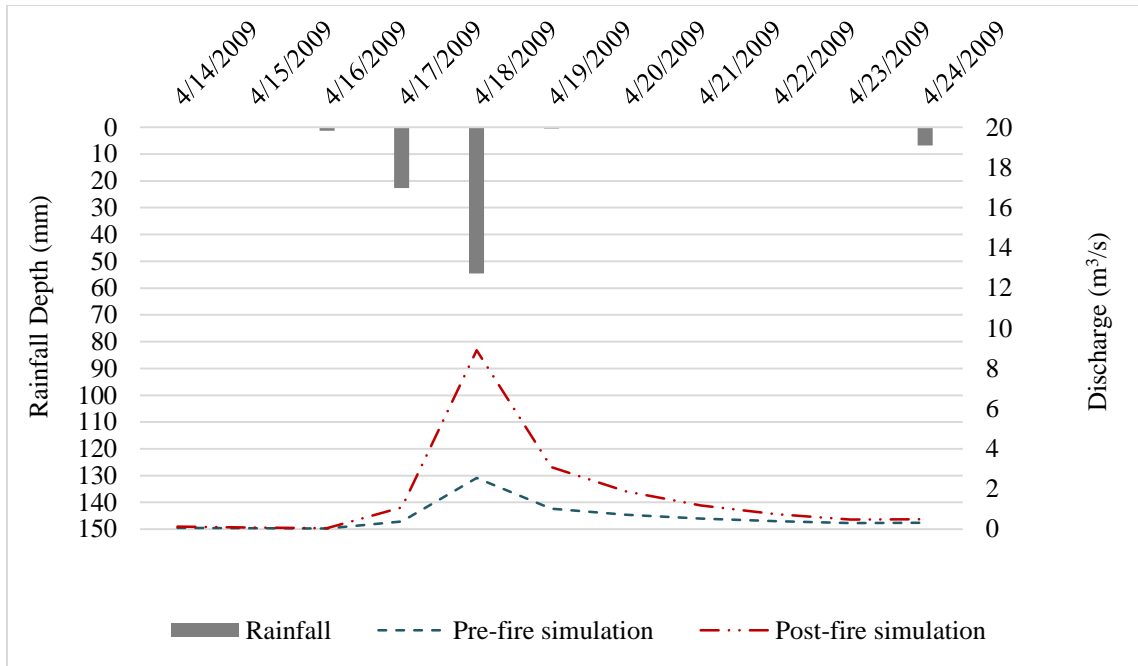


Figure 19a. Water yield generated by a 55 mm (2.15 in) rain event for the calibration period.

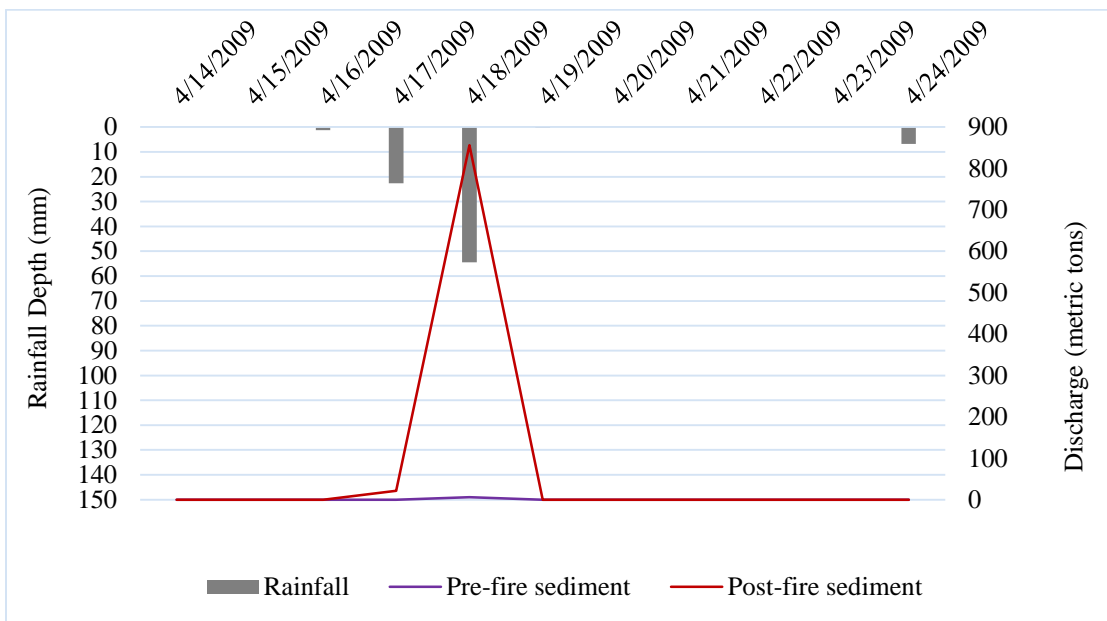


Figure 19b. Sediment yield generated by a 55 mm (2.15 in) rain event for the calibration period.

The pre- and post-fire simulation for the 83 mm (3.29 in) rain event produced a 96% difference ($23.4 \text{ m}^3/\text{s}$) in pre- and post-fire surface water yield. The t-test resulted with a $t = 1.75$ ($p = 0.12$) (Figure 20a). The p value failed to reject the null hypothesis. Sediment yield resulted in a 4,710% difference (7,771.06 metric tons) and a t-test of $t = 1$ ($p = 0.35$) (Figure 20b). The p value failed to reject the null hypothesis.

Table 12. Subbasin 4 simulation totals for pre- and post-fire peak rainfall intensity, time to peak (T_p), peak discharge (Q_p), runoff volume, and sediment volume for the 83 mm (3.29 in) rain event.

Figure	Date of Event	Peak Rainfall Intensity	Simulation	Q_p , m^3/s	T_p , days	Mean Runoff Volume, m^3/s	Total Sediment Yield, Metric Tons
20a, 20b	05/01/2007	83 mm (3.29 in)	Pre-fire	17.45	1	24.33	164.98
			Post-fire	31.61	1	47.74	7936.04

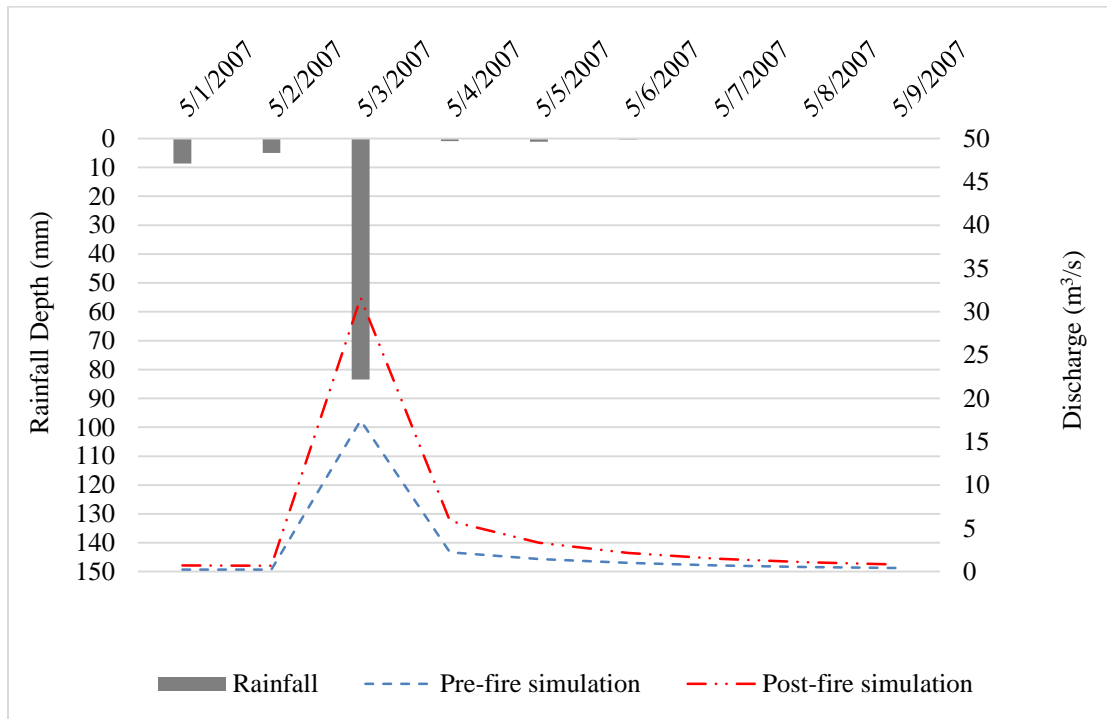


Figure 20a. Water yield generated by an 83 mm (3.29 in) rain event for the calibration period.

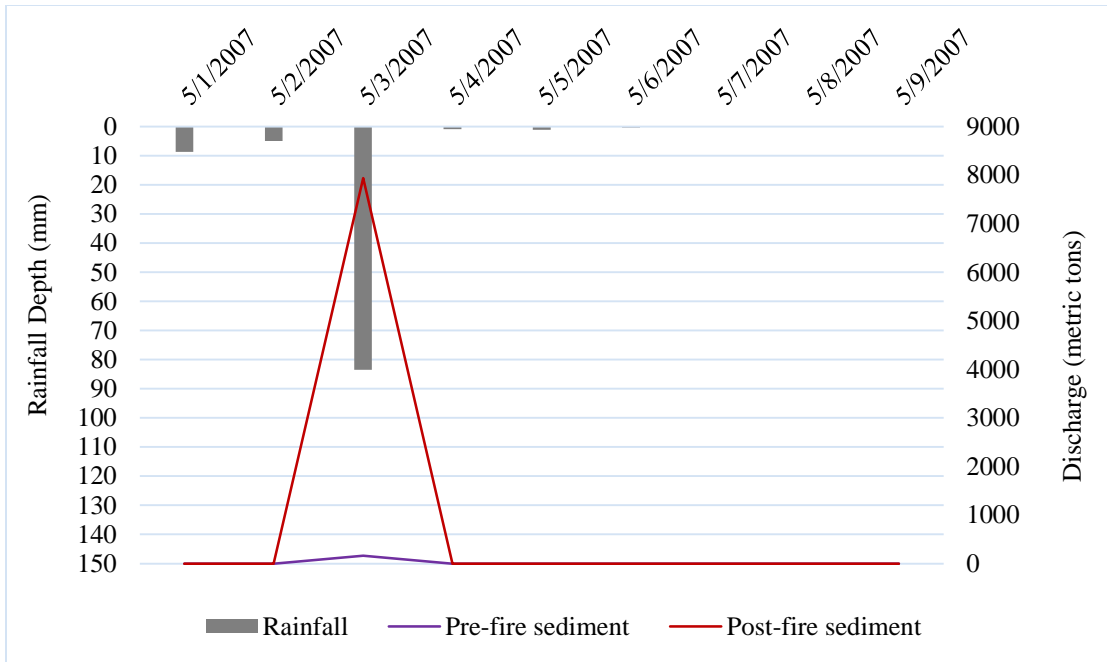


Figure 20b. Sediment yield generated by an 83 mm (3.29 in) rain event for the calibration period.

Finally, the pre- and post-fire simulation for the 25 mm (1 in), 26 mm (1.01 in), 42 (1.66 in) rain events produced an 314% difference (51.17 m³/s) in pre- and post-fire surface water yield (21a), where the Wilcoxon test produced a significant Z score of -4.29 ($p < 0.001$). The hypothesis was rejected for water yield. Sediment yield resulted in an 186,316% difference (8,903.46 metric tons) (21b), and the Wilcoxon test produced a Z score of -0.63 ($p = 0.53$). Similar to the previous discrete events, the p value failed to reject the null hypothesis for sediment yield.

Table 13. Subbasin 4 simulation totals for pre- and post-fire peak rainfall intensity, time to peak (T_p), peak discharge (Q_p), runoff volume, and sediment volume for the multimodal rain event.

Figure	Date of Event	Peak Rainfall Intensity	Simulation	Q_p , m^3/s	T_p , days	Mean Runoff Volume, m^3/s	Total Sediment Yield, Metric Tons
21a, 21b	11/06/2004	42 (1.66 in)	Pre-fire	3.42	1	2.37	4.78
			Post-fire	15.11	1	13.25	8,909.24

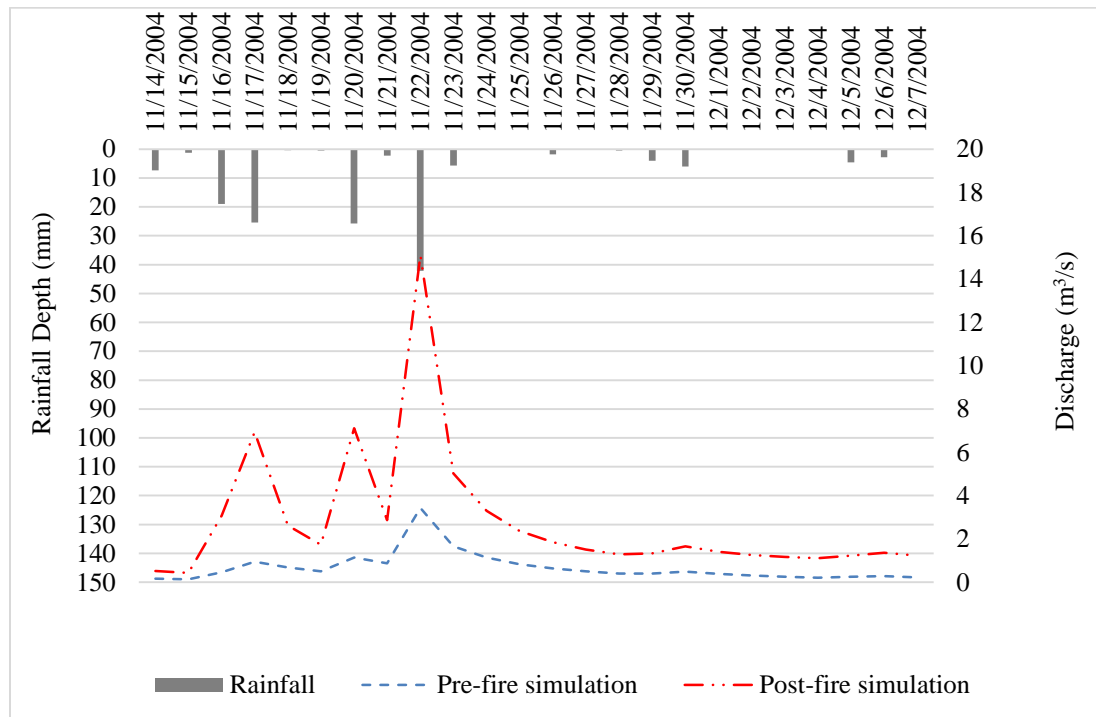


Figure 21a. Water yield generated by 25 mm (1 in), 26 mm (1.01 in), 42 (1.66 in) rain events for the calibration period.

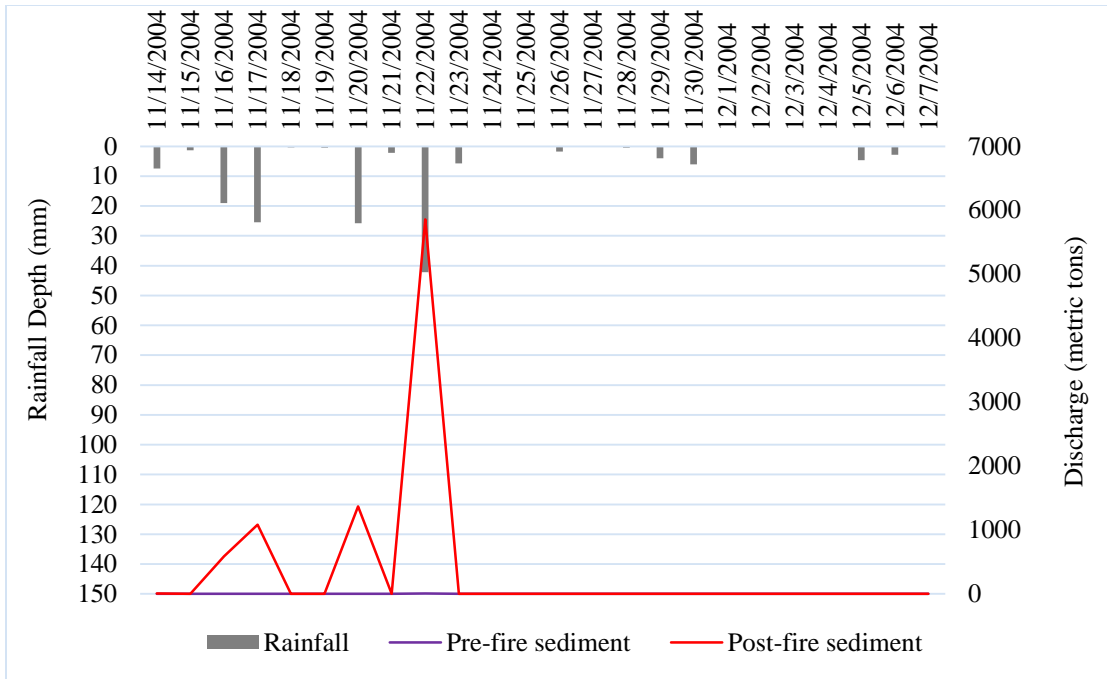


Figure 21b. Sediment yield generated by 25 mm (1 in), 26 mm (1.01 in), 42 (1.66 in) rain events for the calibration period.

5. DISCUSSION

In terms of data input, the pre-fire and post-fire simulations differ by the inclusion of LCLU data that includes the burn scar from the Bastrop Complex Wildfire. The post-fire simulation examined possible changes in stream-flow, and rainfall-runoff response as a direct result of both the LCLU change as well as the severe drought in 2011.

Comparing against the pre-fire simulation, the results of the post-fire simulation in the study area and subbasin 4 consistently produced higher surface water yield, higher sediment yield, and greater instantaneous peak discharge. This trend is consistent for both the continuous streamflow and discrete events. The magnitude of instantaneous peak discharge mostly increased as the magnitude of the rain events increased (e.g., Table 6). With the exception of the 27 mm (1.06 in) (Figure 11a) discrete event from the validation period, time to peak experienced minimal change compared to the pre-fire simulation (e.g., Table 6). In all events, the post-fire sediment yield resulted in greater increases than the surface water yield (e.g., Table 6).

For this study, the pre- and post-fire continuous time simulations were significantly different. However, all discrete events examined in this study failed to reject the null hypotheses. A possible explanation is that the SWAT model is designed for continuous event simulations and its parameters are not sensitive to changes in a single event flood routing. Another possible reason is there are only limited data points in discrete events, which typically have little variation in surface water or sediment yield values in most days except the day after peak discharge. Despite the normal distribution of these rainfall distribution, the small sample (usually n is approximately ten) in all discrete events limit the effectiveness of the t-test in examining any significant

difference. Nevertheless, the statistical tests offered a lens to examine the difference between pre- and post-fire simulation.

5.1 LCLU Change

The post-fire LCLU classification of the study area gained 108.82 square kilometers of the barren class for the October LCLU classification (Table 2). All LCLU classes seemed to have reduced in area after the fire, except for barren and a slight gain in shrub/scrub. As the 2011 Bastrop Complex Fire took place in the loblolly pine forest, it was expected that the evergreen forest area would decrease and a large portion would be reclassified as barren after the wildfire. However, the total area of the evergreen forest did not change much within the study area as the loss was balanced by larger patches in the western portion of the study area (Figure 9). This is more likely a result of LCLU misclassification, than an actual physical change in the composition of LCLU in the study area. Upon inspection of the evergreen forest LCLU class in Google Earth, the October classification seems to include a greater area of mixed pixels in LCLU transition zones; the class also seems to include areas that should be classified as the mixed forest class.

Subbasin 4 gained 65.07 square kilometers of barren land after the fire (Table 3). Besides barren land, subbasin 4 consistently lost area in other LCLU classes, with the exception of the slight gain in shrub/scrub. The loss of 58.57 square kilometers of the evergreen forest in subbasin 4 was caused by the Bastrop Complex Wildfire. The post-fire LCLU change in subbasin 4 indeed confirms the conversion from evergreen forest to barren land due to the Bastrop Complex Wildfire.

The loss of evergreen forest implied a major loss in living photosynthesizing vegetation within the burn scar. Kunze and Stednick (2006) and Townsend and Douglas (2000) discussed the possibility of severe wildfires transforming forests into barren land. While upland vegetation was severely damaged, riparian vegetation appeared to be less damaged and still living (i.e., photosynthesizing) in areas along Alum Creek in the post-fire Landsat imagery (Figure 4). Dwire and Kauffman (2003) stated that microclimate and soil moisture play a role in the differences in wildfire damage severity on upland vegetation as compared to riparian vegetation.

5.2 Hydrology

The hydrologic response is changed as a result of vegetation loss (e.g., evergreen forest) with the replacement of evergreen forest and other vegetation classes by barren land. The hydrologic simulations are calculated using physical variables including canopy storage, soil infiltration, evapotranspiration, transmission loss, and weather parameters such as temperature, precipitation, wind, solar energy, etc. Ambient soil moisture, and the geographic extent, intensity, and duration of precipitation are key factors affecting rainfall-runoff response in a drainage area. The spatial distribution of precipitation plays a role in the accumulation of overland flow, and flood routing gains where rain is falling directly in the stream channel.

5.2.1 Surface Runoff

Surface runoff volume is calculated using the SCS curve number (CN) method. Kunze and Stednick (2006) reported that rainfall intensity and the severity of fire damage are related to increases in surface runoff. It is expected that the post fire

simulation would generate a greater magnitude of surface runoff due to the increase in the total area of barren land cover, which has a lower soil water retention capacity compared to vegetated land cover.

Townsend and Douglas (2004) reported that the increase in post-fire stream flow is inversely proportional to the ratio of vegetation loss within the watershed.

The wildfire transformed 9% of the 1248 square kilometer study area into barren land cover. Compared to contributing drainage area of Colorado River, this wildfire only transformed 0.2% of 75,027 square kilometers (28,968 square mile) into barren land. The hydrologic simulation was trained using the inflow data from the Bastrop gage; therefore the stream flow simulated at the Smithville gage is representative of the entire Colorado River basin upstream of the station. The study area experienced a significant difference in pre- and post-fire surface water yield (12%).

The post-fire discrete event simulations produced greater surface runoff quantity compared to the pre-fire simulations (e.g., Figure 11a). It was found that the post-fire runoff volume increases positively with the magnitude of the rainfall event, however the magnitude of the increase varies.

For the study area, the pre- and post-fire rainfall-runoff simulation of the 27 mm (1.06 in) rain events resulted in a change of 45% ($74.26 \text{ m}^3/\text{s}$) (Figure 11a) during the validation period. Similarly, the 51 mm (2.01 in) rainfall event produced a 61% difference ($129.42 \text{ m}^3/\text{s}$) in surface runoff (Figure 13a). Despite the greater percent increase in runoff volume from 27 mm (1.06 in) to 51 mm (2.01 in) event, the 76 mm (3 in) simulation produced a 46% increase ($279.58 \text{ m}^3/\text{s}$) in surface runoff (Figure 15a).

Nevertheless, the 76 mm (3 in) rain event post-fire runoff volume was indeed greater than the 51 mm (2.01 in) runoff event.

The simulation of Subbasin 4 experienced a higher post-fire increase in net surface water yield compared to the study area for both the discrete and the continuous events. With reference to the pre-fire condition, the post-fire continuous simulation resulted in a 107% increase in stream flow. This is expected because a greater portion of the total area (i.e., 46%) of Subbasin 4 was damaged by the wildfire and transformed into barren land. The post-fire simulation of Subbasin 4 seems to have experienced a decrease in base flow as the post-fire simulation produced less stream flow than the pre-fire simulation during the relatively dry periods. The discrete events consistently produced greater runoff volumes as the magnitude of the rain events increased. For the 31 mm (1.22 in) rain event, the surface volume increased 6.8 m³/s, which was a 289% increase (Figure 18a). Similarly, the increase in surface runoff generated by the multimodal event produced a 314% increase (Figure 21a).

5.2.2 Peak Discharge

Post-fire peak discharge would be expected to increase because more land was converted into barren land as discussed in the previous section. With the reduction of vegetation, CN generally increases, contributing to more rainfall excess and a flashier response in the resulting hydrograph. In drainage areas damaged by wildfire, Scott (1993), Friedel (2011), and Kunze and Stednick (2006) all reported increases in peak discharge by a factor of several hundred. Scott (1993) compared peak discharge in watersheds with different vegetation types. He reported 290% and 1110% increase for

forested watersheds. The simulated changes in peak discharge were consistent with previous findings in the literature.

For every discrete event in the study area and Subbasin 4, peak discharge increased as the rainfall event increased in magnitude. Peak discharge was consistently greater for the post-fire simulation in both the study area and Subbasin 4. Peak discharge increased by greater magnitudes for the validation period compared to the calibration periods. Peak discharge for the validation period increased by 132%, 111% and 71% for the 27 mm (1.06 in), 51 mm (2.01 in) and the 76 mm (3in) rain event respectively (Figure 11a, 13a, 15a). The peak discharge increases at a decreasing rate with higher magnitude of rainfall intensity. Peak discharge Subbasin 4 produced a similar trend: 660%, 249%, and 81% for the 31 mm (1.22 in), 55 mm (2.15 in), and 83 mm (3.29 in) rain event respectively (Figure 18a, 19a, 20a). However, the calibration period did not produce this trend: 5%, 3%, 7% increase for the 31 mm (1.22 in), 55 mm (2.15 in), and 83 mm (3.29 in) rain event respectively (Figure 10a, 12a, 14a).

5.2.3 Time to Peak

In this study, the time to peak was examined among the discrete events. As SWAT simulates daily hydrologic response, any post-fire change in time to peak would need to be greater than one day in order to be detected. Time to peak for the post-fire simulation did not change compared to the pre-fire simulation, with the exception of the 27 mm (1.06 in) (Figure 11a) (Table 6). In that rainfall event, the post-fire time to peak

occurred on the first day after the rain event while the pre-fire simulation peaked on the second day.

A shorter post-fire time to peak could be attributed to an increase in stream flow velocity, and a decrease in channel roughness. Flow velocity is calculated using the product of hydraulic radius and slope, divided by the Manning roughness coefficient. Loss of vegetation from wildfire results in a decrease in surface roughness, leading to an increase in flow velocity (Ryan *et al.*, 2011). Living riparian vegetation along the Alum Creek (Figure 4) would have retained the CN, and surface roughness from pre-fire conditions.

5.2.4 Sediment

High intensity fires late in the dry season result in large areas of exposed soil (Townsend and Douglas, 2000). Erosion from overland flows, and channel degradation generate high sediment yields (Friedel, 2011). The volume of sediment yield depends on the severity of vegetation loss, the timing of the rain event during post-fire vegetation recovery, the susceptibility of soil erosion, and slope (Gartner *et al.*, 2008; Ouyang *et al.*, 2010; Wei *et al.*, 2010). Mass wasting and debris flows become a concern for areas with slope greater than 30% where vegetation is severely damaged by wildfire (Gartner *et al.*, 2008).

Sediment yield is governed by physical hydrology processes. In SWAT, the erosion component MUSSEL determines the soil erodibility factor based on particle size, organic material, soil structure, and permeability. The MUSSEL equation evaluates the soil plant cover to determine if hydrometeors impact soil at terminal velocity. Vegetation

cover reduces the velocity, and therefore the impact of the rain drops. SWAT updates the vegetative cover daily in order to account for phenological cycle. It accounts for slope, coarse fragments, such as rocks, snow, and terracing or tillage. The MUSEL equation calculates erosive energy from the subbasin area, runoff volume, surface runoff lag, and peak runoff rate. Sediment transport is calculated using deposition, and degradation processes. The two processes are driven by peak channel velocity. Stream velocity entrains sediment, and excess power causes stream degradation.

The post-fire simulation consistently produced higher sediment yield compared to pre-fire sediment yield. The continuous stream flow simulation experienced an increase of 86% for the validation period. Although the percent increase was greater for the calibration period, the validation produced a higher quantity of sediment yield. The validation period simulation produced 445,785 metric tons of sediment, and the calibration period produced 69,740 metric tons of sediment yield.

For the discrete rain events in the study area, the quantity of the sediment yield increased as the magnitude of the rain event increased. The 76 mm (3 in) rain event generated drastic increases in post fire sediment yield. The sediment yield increased from 1508 metric tons to 19,902.72 metric tons (1,220% increase) (Table 8, Figure 15b), and the surface runoff increased by 278.58 m³/s (46% increase). Constant with the study area, the sediment yield in subbasin 4 experienced an increase as the magnitude of the rain events increased. When compared to the sediment yield simulated for same rain events in the study area, the subbasin produced almost as much sediment (659.91 metric tons) (Table 10) as the study area (660.6 metric tons) (Table 6) for the 31 mm (1.22 in) rain event. As the magnitude of the rain events increase, we see the study area produce a

greater difference in the quantity of sediment yield, e.g., for the 55 mm (2.15 in) rain event the study area produced 1,090.63 metric tons (Table 7) of sediment, and subbasin 4 produced 877.37 (Table 11) metric tons of sediment.

The multimodal rain events produced substantial increases in sediment yields as well. The multimodal event produced a 315% (5,186.69 metric tons) increase in sediment yield, a 1% (38.85 m³/s) increase in surface runoff, and peak discharge increased from 168.4 m³/s to 169.4 m³/s.

These results suggest that barren LCLU, soil type, and other physical characteristics of the drainage area play a big role in the increase in sediment yield compared to surface yield and stream velocity. When the surface runoff increased substantially, there was an enormous rise in sediment yield.

5.2.5 Comparing the Calibration and the Validation Period Simulation Results

In general, the validation period experienced a greater increase in surface water yield compared to the calibration period. However, the magnitude of the change in sediment yield was generally more consistent with the calibration period. This could be explained by many factors. Land cover data was acquired by Landsat 5 in 2011, and the validation time period ranged from 1998-2004. The predictive abilities of continuous simulations are generally expected to decrease for time periods that do not have temporally consistent with the land cover data; particularly in watersheds that have experienced land cover change over the duration of the SWAT simulation (Lee *et al.*, 2011). The portion of the continuous simulation that is temporally consistent with all of the input data, including land cover, is generally selected for calibration in order to

maximize calibration results, therefore the objective functions are expected to be weaker for the validation period, and strongest for the calibration period (Lee *et al.*, 2011).

Unfortunately, the sediment yield was not calibrated due to the lack of available data.

5.3 Limitations

In order for the SWAT model to be considered a suitable predictive tool, the comparison of simulation and observed stream flow must meet the required objective functions (i.e., NSE and R^2). The objective function results for both the calibration and validation periods were very strong and indicated that the pre-fire simulation can be considered a very good predictor. However, the National Centers for Environmental Prediction (NCEP) Climate Forecast System Reanalysis (CFSR) weather data range available for this study was limited to 1979-2010, which restricted the simulation time period. The full simulation (including SWAT model warm-up time period) runs from 1990 to 2010. Because the simulation ends in 2010, the only post fire (i.e., October 2011) data used in this analysis is the post-fire LCLU data. The pre- and post-fire LCLU data is the only data set that differentiates the pre-and post-fire SWAT simulations. Because of data limitations, this study did not use post-fire observed stream flow data to verify the post-fire simulations. The results of this study should be considered a simulation exercise to examine a range of hydrology conditions in a post-fire scenario.

The predictive abilities of the calibrated and validated continuous stream flow simulations are considered strong (Moriassi, 2006). Discrete storm flow events were extracted from the continuous stream flow record for analysis and to explore the relationship between rainfall intensity and post-fire hydrologic response. For some

calibrated discrete storm events, the simulated values do not meet the required objective functions. Therefore, the predictive abilities of these discrete storm flow events are questionable. Moreover, and the temporal resolution of the stream flow data are limited to daily values, and thus there is not enough temporal granularity to refine the precise timing of the pre- and post-fire storm flow peaks (e.g. in hours or minutes). The SWAT model is designed for land cover management scenario analysis of long-term continuous event simulation, making it less ideal for the simulation of single event flood routing (Neitsch, *et al.*, 2011). Despite the normal distribution of the discrete events, the low sample size (with n of approximately ten) biases the t-test towards insignificance, while the small initial measurement greatly amplifies percent difference, could explain the unusual result of enormous percent increase (e.g., twelve-fold in sediment yield of figure 15b) that does not meet statistical significance.

The comparison of pre- and post-fire LCLU classification indicated that there were inconsistencies in the labeling of spectral classes. For example there was a 0.7 loss in the evergreen forest for the study area, whereas the subbasin 4 lost 58.57 square kilometers of evergreen forest as a result of the wildfire. LCLU classification resulted in moderate agreement for the class assignment of the LCLU type. The remote sensing LCLU classification was conducted during the driest period recorded in Texas history, after the landscape had endured the hottest temperatures recorded in Texas history. Comparing the August image to the October image, barren land cover increased throughout the study area. It is important to point out that the differences in the hydrologic outputs are sensitive to land cover. Hence, the combined results from LCLU

changes could be caused by the Bastrop Complex Wildfire, the extreme drought condition of 2011, and/or LCLU classification inconsistency.

A limitation of the SWAT model is the over simplification of physical processes. Additionally, the classification of the wildfire burn scar as barren could be an oversimplification of the transformation that the burned LCLU experienced. It should be noted that the burn scar is expected to recover as vegetation grows back; therefore the hydrological conditions simulated in this study are limited to the post-fire and pre-burn scar recovery time period.

6. CONCLUSION

The Bastrop Complex Wildfire of September 2011 proved to be one of the most destructive wildfire in Texas history. The wildfire consumed vegetation that endured the hottest, and driest periods recorded in Texas history. Remote sensing land cover classification using imagery from August and October 2011 captured the stressed landscape, and quantified LCLU change caused by the wildfire.

The comparison of pre-fire hydrology simulation to the post-fire scenario revealed changes in surface hydrology. The continuous simulation resulted in an increase in surface runoff, and sediment yield. Despite the results of the unimodal rainfall events not being statistically significant, there was a consistent trend of increasing post-fire peak discharge that is positively related to the magnitude of the rainfall events. In contrast, the discrete rainfall events produced a greater post-fire runoff volume, but not necessarily positively associated with the magnitude of the rain event. These findings suggested that other physical factors (e.g., the geographic distribution of precipitation, and ambient soil moisture conditions) played important roles in determining the magnitude of the increase of the surface runoff. The post-fire time to peak remained unchanged compared to the pre-fire simulation, with the exception of one rainfall-runoff event that decreased by one day. The post-fire sediment yield generated the greatest differences between the pre and post-fire simulation.

The results of the hydrology simulated in this study represent a stressed and damaged landscape. As the vegetation recovers from the drought and the wildfire, the

hydrology will gradually recover. The regrowth and regeneration of the Lost Pine Forest could take decades.

6.1 Future Research Opportunities

There are many opportunities for future research. Over time there will be enough observed data collected, via remote sensing systems and streamflow gauging, to verify the results of this simulation; observed streamflow rainfall-runoff response from before and after the Bastrop Complex Wildfire can be directly compared. Additional hydrologic data can be used to examine the long-term impact of the wildfire on hydrology. Future research could examine the effects of fire on geomorphology within the watershed, and the role geomorphic changes have on hydrology in the watershed. As the Loblolly Pine forest is replanted, and the vegetation within the watershed recovers over the next 30 years, science will have the opportunity to examine the relationship between the long-term vegetation recovery and hydrology within the watershed, i.e., the ecological resilience of the Lost Pine Forest.

7. LITERATURE CITED

- Abbaspour, K.C., J. Yang, I. Maximov, R. Siber, K. Bogner, J. Mieleitner, J. Zobrist, and R. Srinivasan, 2007. Modelling hydrology and water quality in the pre-alpine/alpine Thur watershed using SWAT, *Journal of Hydrology*, 333: 413–430.
- Alemaw, B.F., and T.R. Chaoka, 2003. A continental scale water balance model: a GIS-approach for Southern Africa, *Physics and Chemistry of the Earth*, 28: 957–966.
- Al-Sabhan, W., M. Mulligan, and G.A. Blackburn, 2003. A real-time hydrological model for flood prediction using GIS and the WWW, *Computers, Environment and Urban Systems*, 27: 9–32.
- Arnold, J.G., 2012. SWAT: Model Use, Calibration, and Validation, *Soil & Water Division of ASABE*, 55: 1491-1508.
- Benda, L., D. Miller, P. Bigelow, and K. Andras, 2003. Effects of post-wildfire erosion on channel environments, Boise River, Idaho, *Forest Ecology and Management*, 178: 105–119.
- Cannon, S.H., J.E. Gartner, R.C. Wilson, J.C. Bowers, and J.L. Laber, 2008. Storm rainfall conditions for floods and debris flows from recently burned areas in southwestern Colorado and southern California, *Geomorphology*, 96: 250– 269.
- Chander, G., B.L. Markham, and D.L. Helder, 2009. Summary of current radiometric calibration coefficients for Landsat MSS, TM, ETM+, and EO-1 ALI sensors, *Remote Sensing of Environment*, 113: 893–903.
- Doerr, S.H., and R.A. Shakesby, 2006. Forest fire impacts on catchment hydrology: A critical review, *Forest Ecology and Management*, 234S: S161.
- Dwire, K.A., and J.B. Kauffman, 2003. Fire and riparian ecosystems in landscapes of the western USA, *Forest Ecology and Management*, 178: 61– 74.
- Friedel, M.J., 2011. Modeling hydrologic and geomorphic hazards across post-fire landscapes using a self-organizing map approach, *Environmental Modelling & Software* , 26: 1660– 1674.
- Gartner, J.E., S.H. Cannon, P.M. Santi, and V.G. Dewolfe, 2008. Empirical models to predict the volumes of debris flows generated by recently burned basins in the western U.S. *Geomorphology* , 96: 339– 354.

- Gassman, P. W., Reyes, M. R., Green, C. H., Arnold, J. G., 2007. The Soil and Water Assessment Tool: Historical Development, Applications, and Future Research Direction, *Soil & Water Division of ASABE*, 50(4): 1211–1250.
- Jat, M.K., 2009. Remote sensing and GIS-based assessment of urbanization and degradation of watershed health, *Urban Water Journal*, 6.3: 251– 263.
- Kinoshita, A.M., and T.S. Hogue, 2011. Spatial and temporal controls on post-fire hydrologic recovery in Southern California watersheds, *Catena*, 87: 240–252.
- Kunze, Matt D., Stednick, John D., 2006. Streamflow and suspended sediment yield following the 2000 Bobcat fire, Colorado, *Hydrological Processes*, 20: 1661–1681.
- Lee, T., R. Srinivasan, J. Moon, and N. Omani, 2011. Estimation of Fresh Water Inflow to Bays From Gaged and Ungaged Watersheds, *American Society of Agricultural and Biological Engineers*, 27(6): 917-923.
- Loaiciga, Hugo A., Pedreros , Diego, Roberts, Dar, 2001. Wildfire-streamflow interactions in a chaparral watershed, *Advances in Environmental Research*, 5: 295– 305.
- Moody, J.A., D.A. Martin, and S.H. Cannon, 2007. Post-wildfire erosion response in two geologic terrains in the western USA, *Geomorphology*, 95: 103– 118.
- Moradkhani, H., R.G. Baird, and S.A. Wherry, 2010. Assessment of climate change impact on floodplain and hydrologic ecotones, *Journal of Hydrology*, 395: 264–278.
- Moriasi, D. N.: *et al.*, 2007. Model Evaluation Guidelines For Systematic Quantification of Accuracy in Watershed Simulations, *Soil & Water Division of ASABE*, SW 50(3): 885– 900.
- NASA, 2011. Landsat 7 Science Data Users Handbook, URL: <http://landsathandbook.gsfc.nasa.gov/sysper/>, NASA (last date accessed: 23 November 2013).
- National Drought Mitigation Center (NDMC), 2011. U.S. Drought Monitor, Texas, September 6, 2011, URL: droughtmonitor.unl.edu/archive.html, U.S. Department of Agriculture (USDA), and the National Oceanic and Atmospheric Administration (NOAA) (last date accessed: 03 August 2013).
- Nie, W., Y. Yuan, W. Kepner, M.S. Nash, M. Jackson, and C. Erickson, 2011. Assessing impacts of Landuse and Landcover changes on hydrology for the upper San Pedro watershed, *Journal of Hydrology*, 407: 105–114.

- Neitsch, S.L., J.G. Arnold, J.R. Kiniry, and J.R. Williams, 2011. Soil and Water Assessment Tool Theoretical Documentation Version 2009, *Texas Water Resources Institute Technical Report No. 406*.
- Ouyang, W., F. Hao, A.K. Skidmore, and A.G. Toxopeus, 2010. Soil Erosion and Sediment yield and their relationships with vegetation cover in upper stream of the Yellow River, *Science of the Total Environment*, 409: 396–403.
- Pisinaras, V., C. Petalas, Gikas, Georgios D., Gemitzi, Alexandra, and V. A. Tsihrintzis, 2010. Hydrological and water quality modeling in a medium-sized basin using the Soil and Water Assessment Tool (SWAT), *Desalination*, 250: 274–286.
- Reistetter, J.A., and M. Russell, 2011. High-resolution land cover datasets, composite curve numbers, and storm water retention in the Tampa Bay, FL region, *Applied Geography*, 31(2): 740– 747.
- Ridenour, K., Rissel, S., Wade, P., Gray, R., Fisher, M., and Sommerfeld, J., 2012, *Bastrop Complex Wildfire Case Study*, Texas Forest Service and Bastrop County office of Emergency Management, 205 p.
- Ryan, S.E., K.A. Dwire, and M.K. Dixon, 2011. Impacts of wildfire on runoff and sediment loads at Little Granite Creek, western Wyoming, *Geomorphology*, 129: 113– 130.
- Santi, P.M., V.G. Dewolfe, J.D. Higgins, S.H. Cannon, and J.E. Gartner, 2008. Sources of debris flow material in burned areas, *Geomorphology*, 96: 310– 321.
- Scott, D.F., 1993. The hydrological effects of fire in South African mountain catchments, *Journal of Hydrology*, 150: 409–432.
- Shakesby, R.A., and S.H. Doerr, 2006. Wildfire as a hydrological and geomorphological agent, *Earth-Science Reviews*, 74: 269– 307.
- Shen, Z.Y., L. Chen, Q. Liao, R.M. Liu, and Q. Huang, 2013. A comprehensive study of the effect of GIS data on hydrology and non-point source pollution modeling, *Agricultural Water Management*, 118: 93–102.
- Soil Conservation Service, 1986. *Urban Hydrology for Small Watersheds. Tech. Release No. 55.*, U.S.D.A., Washington D.C.
- Texas Parks and Wildlife Department (TPWD), 2011. Bastrop County Complex Wildfire; ~33,284 acres., URL: <http://www.tpwd.state.tx.us/spdest/findadest/parks/bastrop/fire/> (last date accessed: 08 August 2013).

- Townsend, S.A., and M.M. Douglas, 2000. The effect of three fire regimes on stream water quality, water yield and export coefficients in a tropical savanna (northern Australia), *Journal of Hydrology*, 229: 188– 137.
- Townsend, S.A., and D. Douglas Michael M., 2004. The effect of a wildfire on stream water quality and catchment water yield in a tropical savanna excluded from fire for 10 years (Kakadu National Park, North Australia), 38: 3051– 3058.
- U.S. Census Bureau, 2014. State & County Quick Facts: Bastrop County,
URL: <http://quickfacts.census.gov/qfd/states/48/48021.html> (last date accessed: 2 April 2014).
- U.S. Geological Survey, 2014a. USGS 08159200 Colorado Rv at Bastrop, TX,
URL: http://waterdata.usgs.gov/nwis/nwisman/?site_no=08159200&agency_cd=USGS, National Water Information System (last date accessed: April 6 2014).
- U.S. Geological Survey, 2014b. USGS 08159500 Colorado Rv at Smithville, TX,
URL: http://waterdata.usgs.gov/nwis/nwisman/?site_no=08159500&agency_cd=USGS, National Water Information System (last date accessed: April 6 2014).